Therapeutic Exploration of FDA-Approved Small Molecules for Fragile X-Associated Tremor/Ataxia Syndrome (FXTAS)

M.Sc. Thesis

By

RITIKA RAWAT

DEPARTMENT OF BIOSCIENCES AND BIOMEDICAL ENGINEERING

INDIAN INSTITUTE OF TECHNOLOGY INDORE

MAY 2025

Therapeutic Exploration of FDA-Approved Small Molecules for Fragile X-Associated Tremor/Ataxia Syndrome (FXTAS)

A THESIS

Submitted in partial fulfilments of the

requirements for the award of the degree

of

Master of Science

by

RITIKA RAWAT

DEPARTMENT OF BIOSCIENCES AND BIOMEDICAL ENGINEERING

INDIAN INSTITUTE OF TECHNOLOGY INDORE

MAY 2025

INDIAN INSTITUTE OF TECHNOLOGY INDORE

CANDIDATE'S DECLARATION

I hereby certify that the work which is being presented in the thesis entitled 'Therapeutic exploration of FDA approved small molecules for Fragile-X-associated Tremor/Ataxia Syndrome (FXTAS)' in the partial fulfilment of the requirements for the award of the degree of **Master's of Science**, and submitted in the Department of Biosciences and Biomedical Engineering, **Indian Institute of Technology Indore**, is an authentic record of my own work carried out during the time period July, 2022 to May, 2024 under the supervision of **Prof. Amit Kumar.**

The matter presented in this thesis has not been submitted by me for the award of any other degree of this or any other institute.

Ritika 22/5/25

Signature of student (with date)

Ritika Rawat

This is to certify that the above statement made by the candidate is correct to the best of my/our knowledge.

Signature of the Supervisor of M.Sc. thesis (with date)

21.05.2025

Prof. Amit Kumar

Ritika Rawat has successfully given his M.Sc. Oral Examination held on 5th May 2025.

Signature of the Supervisor of the MSc thesis

Date: 21.05.2025

P.V. Hodgire

Convener, DPGC

Date: 22/05/2025

Acknowledgements

The completion of my Master's thesis was made possible due to the efforts, help, and guidance of many, and I would like to thank and acknowledge everyone in this section. Firstly, I would like to thank my guide, Prof. Amit Kumar, for providing me with the opportunity to work on this project and for providing me with invaluable support, constructive feedback, and guidance throughout this journey. I extend my thanks to the head and faculty of the Department of Biosciences and Biomedical Engineering (BSBE) for their immense support.

My lab members have been a constant source of support, motivation, and love for me. I would like to particularly thank Mr. Krishna Singh Solanki and Ms. Sakshi Shukla; without them, this project would not be possible. Their enthusiasm and involvement in my project made this journey fairly easy. I would like to extend my gratitude to other lab members, Ms. Kumari Aditi Pramod, Ms. Shubhi Khandelwal, Mr. Soumalya Das, Ms. Mansee Patel, Mr. Ashmad Nayak, Ms. Pronamika Chetia, Mr. Aritra Chakraborty, Ms. Priya Gupta, and Ms. Aakriti Singh for their thoughtful scientific inputs and support.

On a personal level, I am grateful to my friends at IIT Indore, Ms. Sanjana Kumari and Ms. Chaitali Vora, for the mental and emotional support and guidance. Lastly, without whom none of this would be possible. I thank my Parents, Mr. Puran Singh Rawat, Ms. Leela Rawat, and my siblings, Ms. Jaya Rawat and Mr. Jai Rawat, for always believing in me, providing me with everything, and for the love and care.

Dedicated to my Family

Abstract

From a drug repurposing perspective, targeting neurological disorders like Fragile X-associated Tremor/Ataxia Syndrome (FXTAS) offers both urgency and opportunity. FXTAS, a late-onset neurodegenerative disorder caused by CGG trinucleotide repeat expansion in the *FMR1* gene, remains without an effective treatment. The toxic RNA gain-of-function from expanded repeats leads to RNA foci formation, splicing defects, and polyglycine (FMRpolyG) protein aggregation, contributing to progressive neuronal dysfunction. This thesis explores the repurposing of FDA-approved small molecules to selectively bind r(CGG)exp RNA and mitigate its downstream pathological effects.

Using a multifaceted approach, the project combined biophysical studies, cell-based assays, and an in vivo *Drosophila melanogaster* model to evaluate therapeutic efficacy. Biophysical characterization revealed a strong and specific interaction between the candidate molecule and CGG repeat RNA, altering its structure and reducing RNA-protein complex formation. In HEK-293 and COS-7 cells expressing expanded CGG repeats, the compound demonstrated promising cellular rescue, diminishing RNA foci, correcting splicing errors, and reducing FMR polyG aggregates.

However, these encouraging results did not translate into neuroprotection in the *Drosophila* disease model. Despite proper delivery and experimental validation, the treated flies showed no significant improvement in locomotor performance, as assessed through negative geotaxis and flight assays. Western blotting further confirmed the absence of reduction in FMR polyG protein levels, suggesting limited in vivo efficacy in this model.

In conclusion, while the study validates the molecular and cellular potential of RNA-targeting small molecules in FXTAS, it also highlights the challenges in bridging the gap from bench to behavior. Future work must focus on optimizing compound bioavailability,

exploring synergistic treatment combinations, and testing in higher-order animal models. This thesis underscores the importance of integrated models in drug repurposing for neurodegenerative diseases, where success in vitro does not always guarantee impact in vivo, but every step brings us closer to hope.

Keywords: FXTAS, CGG, Poly-G, *Drosophila melanogaster*, small molecules

Publications

Publication from thesis:

Repurposing Drug P5 for FXTAS: Ineffective Against RNA-Mediated Neurodegeneration.

(Manuscript under preparation)

Publication apart from thesis:

Soumalya Das, Mansee Patel, Shubhi Khandelwal, Ritika Rawat, Sakshi Shukla, Aditi Pramod Kumari, Krishna Singh, Amit Kumar *.From Mutations to Microbes: Investigating the Impact of the Gut Microbiome on Repeat Expansion Disorders. Journal of Neurochemistry.

(Manuscript ID: JNC-2025-0291) *(under review)*

Table of contents

1- List of Figures

2- Nomenclature

3- List of Acronyms

4- **Chapter 1- Introduction**

5- **Chapter 2- Literature Review and Problem Formulation**

6- **Chapter 3- Materials, methods, and instrumentation**

3.1 : Materials

3.2 : RNA oligo synthesis using T7 RNA Polymerase mediated in vitro transcription reaction

3.2.1 : Expression and purification of T7 RNA polymerase

3.2.2 : Polymerase chain reaction amplification

3.2.3 : *In vitro* transcription reaction

3.3 : Fluorescence Binding Assay

3.4 : Circular Dichroism Spectroscopy

3.5 : CD melting

3.6 : Electrophoretic Mobility Shift Assay

3.7 : PCR stop assay

3.8 : NMR Spectroscopy

3.9 : Assessment of the Canonical GFP and Non-canonical FMR1 polyG-GFP Protein Aggregates using Fluorescence Microscopy

3.10 : Quantification of RAN Translation by Western blot

3.11 : Improvement of splicing defects in the cellular model

3.12 : MitoSOX™ Red Staining in COS-7 Cells

3.13 : TMRM Staining in COS-7 Cells

3.14 : Rough eye phenotype assessment

3.15 : Drosophila Climbing assay

3.16 : Larval Crawling assay

3.17 : Drosophila Flight assay

3.18 : Quantification of RAN Translation by Western blot

7- **Chapter 4- Results**

4.1: Fluorescence Binding Assay

4.1.1 : Fluorescence Binding Assay of P5 with 11 loop mismatch library

4.1.2 : Fluorescence Binding Assay of P5 with control RNA

4.1.3 : Fluorescence Binding Assay of P5 with control DNA

4.1.4 : Fluorescence Binding Assay of P5 with expanded r(CGG) repeats

4.2: Circular Dichroism Spectroscopy

4.3: CD Melting

4.4: Electrophoretic Mobility Shift Assay

4.5: PCR stop assay

4.6: NMR spectroscopy

4.7: Poly G aggregate visualisation

4.8: Quantification of RAN Translation by Western Blot

4.9: Improvement of splicing defects in the cellular model

4.10: MitoSOX™ Red Staining in COS-7 Cells

4.11: TMRM Staining in COS-7 Cells

4.12: Rough eye phenotype assessment

4.13: Drosophila Climbing Assay

4.14: Larval Crawling assay

4.15: Drosophila Flight assay

4.16: Quantification of RAN Translation by Western blot

8- Chapter 5: Discussion

9- Chapter 6: Conclusion and future perspective

10- References

List of Figures

Fig. 1.1- Schematic representation of the pathogenic mechanism of FXTAS.

Figure 2.1: Schematic representation of potential therapeutics for FXTAS using small molecule drug targets.

Figure 3.1: Jablonski's diagram of the fluorescence phenomenon.

Figure 3.2: Schematic representation of Electrophoretic mobility shift assay.

Figure 3.3: Schematic representation of the occurrence of splicing defects in FXTAS.

Figure 4.1: Bar graph representing Kd values of the library of 14 small molecule with $(CGG)_6$ repeat RNA.

Figure 4.2: PubChem structure of P5.

Figure 4.3: Plots of fluorescence titration of P5 with 11 RNA sequences with 1x1 internal RNA motif.

Figure 4.4: Evaluation of molecule P5 using fluorescence binding assay one-mode curve fitting of 11 RNA sequences containing 1x1 internal loop with P5.

Figure 4.5: Evaluation of molecule P5 using fluorescence binding assay one mode curve fitting of extended r(CGG) RNA with P5.

Figure 4.6: Plots of fluorescence titration of P5 with different DNA/RNA controls.

Figure 4.7. Circular dichroism spectroscopy titration of r(CGG)exp and r(AU)exp duplex RNAs in the presence of P5.

Figure 4.8: A systemic representation of the thermal denaturation profile of r(CGG)exp RNAs with P5.

Figure 4.9: Gel retardation assay. The gel images shows that an increasing concentration of P5 significantly retards the mobility of CGG repeat RNAs over AU duplex RNA.

Figure 4.10: PCR stop assay. Gel images show the decreased intensity of PCR product with increasing concentration of P5 compared with AU paired template.

Figure 4.11: Represents NMR peak broadening upon titration of P5 with (CGG)6 RNA.

Figure 4.12: (a.) Images represent the FMR1polyG-GFP inclusions in r(CGG)x99-EGFP expressing COS7 cells with P5 at different concentrations.

Figure 4.13: Immunoblots representing inhibition of FMR polyG protein aggregates for 24 h in the presence of P5, whereas no significant difference was seen in the concentration of protein controls.

Figure 4.14: (a.) Schematic representation of splicing defects associated with the SMN2 (Survival of Motor Neuron 2) gene and Bcl-x (B-cell lymphoma extra large) gene in FXTAS. (c.) Gel images and graphs illustrate that P5 corrects the SMN2 defects in relation to their concentration.

Figure 4.15: Fluorescence microscopy images of Cos7 cells after Mitosox staining. Accompanying Bar graph denoting percentage of Mitosox signal intensity.

Figure 4.16: Fluorescence microscopy images of Cos7 cells after TMRM staining. Accompanying Bar graph denoting percentage TMRM signal intensity.

Figure 4.17: (a.) SEM, Light microscopic, and confocal images of the eyes of GMR-Gal4 > UASEGFP flies treated with different concentrations of P5.

Figure 4.18: Crawling assay results for third-instar larvae (Elav-Gal4 > UAS-(CGG)90-EGFP) treated with P5 assessing motor coordination and function.

Figure 4.19: Climbing Assay for Elav-Gal4 > UAS-(CGG)90-EGFP adult flies following the treatment with P5.

Figure 4.20: Schematic results of Drosophila flight assay. Accompanying area plot graphs indicate the number of flies at different heights of the flight chamber.

Figure 4.21: Immunoblots representing levels of Poly-G post drug treatment in Drosophila FXTAS model.

Nomenclature

Λ	Wavelength
ε	Extinction coefficient
℃	Degree centigrade
Δ	Delta
µL	Microlitre
mL	Millilitre
nm	Nanometer
nM	Nano Molar
µM	Micro Molar
M	Molar
s	Seconds
min	Minutes
hr	Hour

Acronyms

CD	Circular Dichroism
FBA	Fluorescence Binding assay
D/N	Drug/Nucleic Acid
DMSO	Di methyl sulfoxide
EDTA	Ethylenediaminetetraacetic acid
EMSA	Electrophoretic Mobility Shift Assay
LB	Luria Broth
PAGE	Polyacrylamide gel electrophoresis
PCR	Polymerase Chain Reaction
PDB	Protein Data Bank
RNA	Ribonucleic acid
Kd	Dissociation constant
Ksv	Stern-Volmer Constant
DTT	Dithiothreitol
PMSF	Phenylmethylsulphonyl fluoride
SDS	Sodium dodecyl-sulfate
Ni-NTA	Nickel-Nitrilotriacetic Acid
IPTG	Isopropylthio-β-galactoside
CV	Column Volume
OD	Optical Density
TNR	Trinucleotide repeat

Chapter 1

Introduction

Drug repurposing, or drug repositioning, is an increasingly valued strategy in pharmaceutical research that involves identifying new therapeutic uses for existing drugs. This approach offers an attractive alternative to traditional drug discovery, which often spans over a decade and demands substantial financial investment. By focusing on compounds with already known safety, pharmacokinetics, and toxicity profiles, drug repurposing can significantly shorten development timelines and reduce the risk of failure in later clinical phases. As a result, it has gained momentum in efforts to find treatments for diseases with unmet medical needs, including neurodegenerative disorders, cancer, and rare genetic conditions.

Numerous successful examples highlight the potential of this approach. Thalidomide, once withdrawn due to severe teratogenic effects, has been successfully reintroduced for the treatment of multiple myeloma and complications of leprosy owing to its immunomodulatory effects (Richardson et al., 2002). Another notable case is sildenafil, which was initially developed as an anti-anginal agent. It was later repurposed for erectile dysfunction and pulmonary arterial hypertension after its vasodilatory properties were better understood (Galie et al., 2005). Similarly, minoxidil, originally intended for hypertension, was found to promote hair growth and is now widely used for the treatment of androgenetic alopecia (Messenger & Rundegren, 2004). Valproic acid, a drug commonly prescribed for epilepsy and bipolar disorder, has shown potential in clinical trials for Alzheimer's disease and spinal muscular atrophy, due to its ability to influence histone deacetylase activity and gene expression (Phiel et al., 2001).

The repurposing of these and other drugs has been made more efficient through the integration of computational approaches, such as molecular docking, network pharmacology, and transcriptomic profiling. These tools allow researchers to predict drug-target interactions and identify

novel indications systematically. As our understanding of disease mechanisms expands and access to omics data improves, drug repurposing continues to evolve into a more precise and rational process. This paradigm not only speeds up therapeutic development but also makes use of the vast array of underutilized or shelved compounds already available in pharmaceutical pipelines.

Considering how long it takes and how much it costs to bring a new drug to market, drug repurposing has become especially important in areas where progress has been slow, like in neurodegenerative diseases Despite decades of intensive research, there is still no cure for most neurodegenerative disorders, including Alzheimer's disease (AD), Parkinson's disease (PD), Huntington's disease (HD), and amyotrophic lateral sclerosis (ALS). Current treatments are primarily symptomatic and offer only modest benefits in slowing disease progression or improving quality of life (Cummings et al., 2019; Kalia & Lang, 2015). One of the primary challenges lies in the complex and multifactorial nature of these diseases, which often involve interlinked mechanisms such as protein misfolding and aggregation, oxidative stress, mitochondrial dysfunction, and chronic neuroinflammation (Ramanan & Saykin, 2013; Heneka et al., 2014). Unfortunately, many drugs developed through traditional pipelines have failed in late-stage clinical trials, highlighting the limitations of single-target approaches (Mullard, 2012).

In this context, drug repurposing offers a promising and time-efficient alternative. Since repurposed drugs have already undergone clinical testing for safety, their use in new indications can progress more quickly through regulatory hurdles (Ashburn & Thor, 2004). Moreover, many of these compounds exhibit polypharmacological properties—meaning they act on multiple pathways—which is particularly advantageous for treating diseases as complex as those involving neurodegeneration (Nosengo, 2016). The growing success of repositioned drugs in preclinical models and early clinical trials is gradually shifting the paradigm in neurodegenerative disease research,

providing a realistic and hopeful route toward discovering more effective treatments.

One example is riluzole, a glutamate release inhibitor originally approved for ALS, which has been evaluated for other neurodegenerative diseases including spinocerebellar ataxia and Huntington's disease due to its neuroprotective effects (Doble, 1996; Benatar, 2007). Valproic acid, widely used as an anticonvulsant and mood stabilizer, has shown potential in preclinical and early clinical studies for AD and HD by modulating histone deacetylase activity and promoting neuroprotection (Su et al., 2004; Ferrante et al., 2003). Another compelling example is rapamycin, an mTOR inhibitor used as an immunosuppressant, which has demonstrated promising results in models of Alzheimer's and Parkinson's diseases through its ability to enhance autophagy and reduce toxic protein aggregates (Bové et al., 2011). Minocycline, a tetracycline antibiotic, has also been explored for multiple neurodegenerative diseases due to its anti-inflammatory and anti-apoptotic properties. Although clinical trials have produced mixed results, its wide therapeutic window and brain permeability continue to make it a candidate of interest (Yong et al., 2004). The repositioning of nilotinib, a tyrosine kinase inhibitor used in chronic myeloid leukemia, has attracted attention for Parkinson's and other synucleinopathies due to its potential to promote autophagic clearance of α-synuclein aggregates (Pagan et al., 2016). These examples illustrate how leveraging the pharmacological properties of existing drugs can help address the multifaceted pathology of neurodegenerative diseases, offering hope for faster identification of effective therapies.

10.1. Neurodegenerative disorders

Neurodegenerative diseases, characterized by the progressive and irreversible loss of neurons and their connections in the brain, have become one of the leading causes of disability and death worldwide. These conditions, which include Alzheimer's disease (AD), Parkinson's

disease (PD), and Huntington's disease (HD), not only severely impair an individual's cognitive, motor, and functional abilities but also place an immense burden on families and healthcare systems. According to recent global health reports, the number of people affected by neurodegenerative diseases continues to rise, with estimates predicting that nearly 160 million people will be living with these conditions by 2060, driven largely by the aging population (Armstrong, 2020). While advancements in medicine have successfully reduced mortality from communicable neurological diseases, the number of deaths attributed to neurodegenerative disorders has increased significantly in recent decades, highlighting the pressing need for effective treatments (Mahajan & Patil, 2021).

The spectrum of neurodegenerative disorders is vast, encompassing a wide range of diseases with varying mechanisms and outcomes. However, they share common features, including the gradual accumulation of misfolded proteins such as amyloid-beta, tau, alpha-synuclein, and TDP-43, which aggregate in the brain, triggering inflammation, oxidative stress, and neuronal death (Ross & Poirier, 2004). These proteins form toxic clumps that disrupt normal cellular functions, leading to cognitive decline and motor impairments. Interestingly, the aging process itself is considered the greatest risk factor for many neurodegenerative diseases, with aging being associated with cellular wear and tear, which exacerbates protein misfolding and diminishes the brain's ability to clear these toxic proteins.

(Feigin et al., 2020). Environmental factors, including exposure to neurotoxins, poor diet, and sedentary lifestyles, also contribute significantly to disease development, with recent studies suggesting a growing link between cardiovascular disease, diabetes, and neurodegeneration (Heneka et al., 2014).

In addition to aging and genetics, neuroinflammation and oxidative stress play critical roles in the progression of these diseases. Pro-

inflammatory cytokines and reactive oxygen species (ROS) are increasingly being recognized as pivotal drivers of neurodegenerative pathology, exacerbating neuronal damage and accelerating disease onset (Ramanan & Saykin, 2013). As the disease progresses, the ability of the brain to repair itself diminishes, making it even more vulnerable to the damaging effects of inflammation and oxidative stress. In light of this, research is increasingly focusing on finding ways to mitigate these factors through pharmacological interventions, lifestyle changes, and more targeted therapies that aim to slow or halt the progression of these disorders.

The need for effective treatments has never been more urgent. Current research efforts are focused on understanding the complex interplay between genetic, environmental, and biological factors that contribute to neurodegeneration. A multi-disciplinary approach involving drug development, advanced diagnostic techniques, and personalized medicine holds great promise for alleviating the burden of these diseases. Moreover, strategies like drug repurposing are offering hope, as existing medications can be re-explored for their potential to address the multifaceted pathologies of neurodegenerative diseases more quickly and cost-effectively (Ashburn & Thor, 2004). By integrating new insights into the biology of these diseases with innovative therapeutic strategies, there is hope for improving the quality of life for millions of individuals affected by these devastating conditions.

10.2. Repeat Expansion disorders

Repeat expansion disorders are a unique and devastating group of genetic diseases caused by the abnormal expansion of repetitive DNA sequences within specific genes. Unlike typical mutations that involve single base changes or deletions, these disorders arise when short DNA motifs—often just a few nucleotides long—are repeated far beyond their normal range. This expansion can interfere with normal gene function and lead to a wide spectrum of clinical symptoms, often involving the nervous system. Most of these disorders are inherited in

an autosomal dominant manner, and their severity, as well as age of onset, tends to worsen in successive generations due to a phenomenon known as anticipation, where the repeat size increases in the germline (Orr & Zoghbi, 2007). While some repeat expansion disorders involve pentanucleotide or hexanucleotide repeats (such as in SCA31 or C9orf72-associated ALS/FTD), a well-studied and clinically significant subset includes those caused by trinucleotide repeat expansions.

Trinucleotide repeat expansion disorders are characterized by the unstable repetition of three-nucleotide sequences (e.g., CAG, CGG, GAA) in coding or non-coding regions of genes. Over 40 human disorders are now known to be caused by such expansions (La Spada & Taylor, 2010). The pathogenesis of these diseases varies depending on the location and nature of the repeat. For instance, CAG repeats in coding regions translate into elongated polyglutamine tracts, leading to toxic protein aggregation, as seen in Huntington's disease and several spinocerebellar ataxias (Ross et al., 1997). Conversely, CGG and GAA expansions often occur in non-coding regions, where they disrupt gene expression and RNA processing. In Fragile X-associated Tremor/Ataxia Syndrome (FXTAS), for example, expanded CGG repeats in the 5′ untranslated region of the *FMR1* gene result in a toxic gain-of-function RNA that sequesters RNA-binding proteins and forms intranuclear inclusions (Hagerman & Hagerman, 2016). Similarly, in Friedreich’s ataxia, expanded GAA repeats in the first intron of the *FXN* gene cause heterochromatin formation and transcriptional silencing, leading to mitochondrial dysfunction (Sandi et al., 2014).

These pathogenic mechanisms—whether mediated through toxic proteins, toxic RNA, or transcriptional repression—underscore the complexity of trinucleotide repeat expansion disorders. Their multisystemic effects, progressive nature, and lack of curative therapies make them a pressing area of neurological research. Advances in molecular biology are helping researchers uncover shared mechanisms

across different disorders, offering potential for cross-cutting therapeutic strategies.

10.3. Pathogenic mechanism

The severity of repeat expansion disorders is strongly negatively correlated with the length of the repeats, as longer expansions are typically associated with earlier onset and greater disease severity (Budworth & McMurray, 2013). These disorders arise from four primary pathogenic mechanisms: (a) loss of function due to transcriptional repression, as seen in *Fragile X Syndrome (FXS)*; (b) RNA gain of function through protein sequestration, exemplified by *Myotonic Dystrophy Type 1 (DM1)*; (c) toxic gain of function due to protein aggregation, as in *Huntington's Disease (HD)*; and (d) Repeat-Associated Non-AUG (RAN) translation, identified in diseases like *Spinocerebellar Ataxia Type 8 (SCA8)* (Fiszer & Krzyzosiak, 2013; Malik et al., 2021).

In disorders like *FXS* and *Friedreich's ataxia*, the expansion of CGG and GAA (or TTC) repeats, respectively, causes transcriptional silencing through epigenetic changes, including DNA methylation and heterochromatin formation. This leads to the loss of critical proteins such as FMRP in FXS and frataxin in Friedreich's ataxia, contributing to neurodevelopmental and mitochondrial dysfunction (Al-Mahdawi et al., 2008; Hagerman et al., 2017). In FXS, additional mechanisms including histone H3K9 methylation, triplex DNA formation, and RNA:DNA hybrids exacerbate *FMR1* gene silencing (Colak et al., 2014).

RNA gain-of-function mechanisms are observed in *DM1*, where CUG repeat expansions in the 3′ untranslated region of the *DMPK* gene form RNA foci that sequester RNA-binding proteins such as MBNL1, disrupting alternative splicing and RNA metabolism (Mankodi et al., 2001; Miller et al., 2000). Similar mechanisms are also evident in other disorders like HD, where toxic RNA species are thought to contribute alongside protein-based toxicity (Nalavade et al., 2013).

Toxic gain of protein function is a hallmark of polyglutamine (Poly-Q) diseases, such as *Huntington's Disease* and *Spinobulbar Muscular Atrophy (SBMA)*. Here, CAG repeat expansions within coding sequences produce abnormally long Poly-Q tracts that misfold and aggregate, disrupting cellular homeostasis via impaired mitochondrial function, altered gene expression, and disrupted proteostasis (Zoghbi & Orr, 2000; Ranganathan et al., 2009).

Lastly, RAN translation represents a non-canonical mechanism whereby expanded repeat RNAs are translated in the absence of an AUG start codon, producing dipeptide repeat proteins from multiple reading frames. This process, triggered by stable secondary structures like hairpins, is implicated in *DM1*, *SCA8*, and *C9orf72*-linked ALS/FTD, further broadening the spectrum of toxic molecular species in repeat expansion disorders (Zu et al., 2011; Cleary & Ranum, 2014).

Together, these varied but interconnected mechanisms emphasize the need for tailored therapeutic interventions, as targeting only one pathological feature may be insufficient to halt disease progression.

10.4. FXTAS (Fragile-X-Tremor Ataxia Syndrome)

The expansion of CGG trinucleotide repeats in the 5′ untranslated region (5′-UTR) of the *FMR1* gene is associated with a spectrum of disorders, including *Fragile X-associated Tremor/Ataxia Syndrome (FXTAS)*, *Fragile X Syndrome (FXS)*, and *Fragile X-associated Primary Ovarian Insufficiency (FXPOI)* (Hagerman & Hagerman, 2013; Hagerman et al., 2001). In healthy individuals, the *FMR1* gene typically contains between 5 and 55 CGG repeats. Repeat lengths in the range of 55–200 define the premutation state, which is implicated in FXTAS and FXPOI. When CGG repeat expansions exceed 200, the allele becomes a full mutation, leading to transcriptional silencing of *FMR1* and causing FXS (Oostra & Willemsen, 2009).

FXTAS is a late-onset neurodegenerative disorder that presents with a range of neurological symptoms, including intention tremor, gait ataxia, Parkinsonism, autonomic dysfunction, and cognitive decline or

dementia (Jacquemont et al., 2003). Two major pathogenic mechanisms underlie the disease. The first involves toxic RNA gain of function, where expanded CGG repeat-containing *FMR1* mRNA adopts stable noncanonical secondary structures, such as hairpins with GG 1×1 internal loops (Handa et al., 2003; Sofola et al., 2007). These RNA structures aberrantly sequester RNA-binding proteins, including *DiGeorge syndrome critical region 8 (DGCR8)*, *Sam68*, *hnRNP A2/B1*, and *Muscleblind-like 1 (MBNL1)*, into nuclear RNA foci, thereby impairing pre-mRNA splicing, microRNA processing, and other essential cellular processes (Sellier et al., 2013; Sofola et al., 2007).

The second mechanism involves Repeat-Associated Non-AUG (RAN) translation, a non-canonical process where translation is initiated in the absence of an AUG start codon. In FXTAS, RAN translation of the CGG repeat-containing mRNA results in the production of toxic homopolymeric proteins, such as polyglycine (polyGly) and polyalanine (polyAla) (Todd et al., 2013; Sellier et al., 2017). These abnormal proteins form intracellular inclusions, which accumulate in neurons and astrocytes, disrupting cellular homeostasis and contributing to neurodegeneration. The interplay between toxic RNA sequestration and toxic RAN-derived protein aggregation highlights the complex pathology of FXTAS and emphasizes the need for therapeutic strategies that simultaneously address both RNA and protein-mediated toxicity.

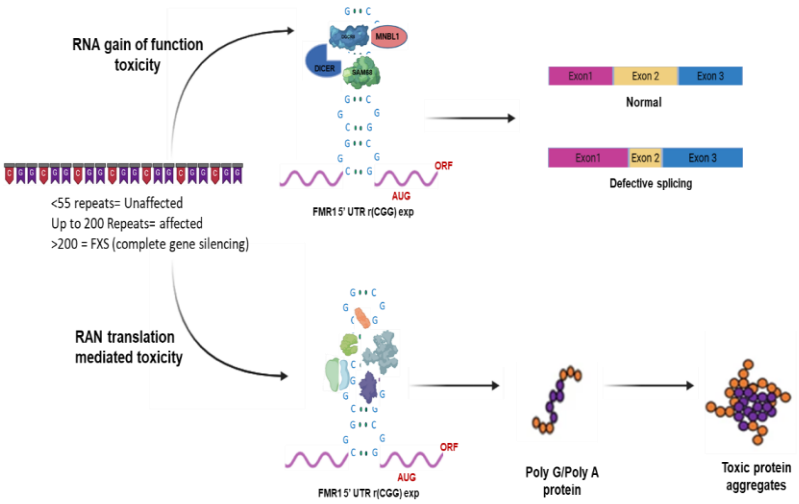

Figure 1.1: Schematic representation of the Pathogenic mechanism of FXTAS.

10.5. Therapeutic Development against Repeat Expansion Disorders

Fragile X-associated Tremor/Ataxia Syndrome (FXTAS) is a debilitating, late-onset neurodegenerative disorder primarily affecting older male carriers of the *FMR1* premutation. Patients typically present with intention tremor, gait ataxia, cognitive decline, autonomic dysfunction, and Parkinsonian features, often resulting in significant loss of independence and quality of life (Jacquemont et al., 2003; Hagerman & Hagerman, 2013). Despite the well-characterized molecular pathology of FXTAS, including toxic RNA gain-of-function and Repeat-Associated Non-AUG (RAN) translation, there are currently no FDA-approved disease-modifying therapies for FXTAS. Treatment remains largely symptomatic and palliative, focused on managing tremor, balance issues, mood disorders, and cognitive symptoms.

Common pharmacological interventions include propranolol and primidone for tremor, levodopa or dopamine agonists for Parkinsonism, and SSRIs or SNRIs for mood symptoms such as

anxiety and depression (Hagerman & Hagerman, 2016). Physical and occupational therapy are essential to support mobility and coordination. In more advanced cases, assistive devices and caregiver support become necessary. However, these treatments do not alter the course of neurodegeneration.

Given the RNA-mediated nature of FXTAS pathology, recent therapeutic strategies have focused on targeting toxic RNA species and preventing protein aggregation. Preclinical studies have investigated antisense oligonucleotides (ASOs) and small molecules that disrupt the CGG repeat hairpin structures or inhibit RAN translation (Todd et al., 2013; Sellier et al., 2017). Some molecules, like TMPyP4 and 1a, have shown potential to bind CGG repeats and reduce RNA foci and protein aggregates in cell and animal models (Krzyzosiak et al., 2012; Simone et al., 2015).

Additionally, drugs like allopregnanolone, a neurosteroid with neuroprotective properties, have shown promise in small clinical trials by improving mitochondrial function and cognition (Wang et al., 2013). Investigational approaches involving RNA interference, gene editing, and RNA-targeted small molecules are being actively explored but remain in early stages of development.

Crucially, there is a growing recognition of the need for personalized, mechanism-targeted therapies in FXTAS, inspired by advances seen in other genetic neurological disorders such as spinal muscular atrophy (SMA). The development of Spinraza (nusinersen) and Zolgensma, both targeting the genetic root of SMA, has offered a blueprint for RNA-based interventions in FXTAS and similar disorders.

As our understanding of the disease mechanisms deepens, especially the interplay between toxic RNA, protein aggregation, and neuroinflammation, novel therapeutic targets are emerging. However, translating these insights into effective treatments will require sustained investment in biomarker development, clinical trial infrastructure, and patient-centered research. For now, FXTAS remains

a poignant example of how genetic knowledge has outpaced therapeutic progress—but also a hopeful one, pointing toward a future where curative or disease-modifying therapies are within reach.

10.6. Therapeutic Development using the *Drosophila* model

Drosophila melanogaster, commonly known as the fruit fly, has been a cornerstone of genetic research for over a century. Despite its diminutive size and evolutionary distance from humans, *Drosophila* shares a remarkable degree of genetic similarity with humans—approximately 77% of human disease-related genes have functional orthologs in the fly genome (Reiter et al., 2001). This conservation makes it an exceptionally powerful model for studying the molecular mechanisms underlying repeat expansion disorders, including Huntington's disease, Fragile X-associated Tremor/Ataxia Syndrome (FXTAS), and various spinocerebellar ataxias.

Several features make *Drosophila* a uniquely tractable model organism:

1. Conserved Genetic Pathways: Key biological pathways such as DNA replication, transcriptional regulation, RNA processing, and protein homeostasis are conserved between *Drosophila* and humans. This conservation allows for meaningful modeling of pathogenic mechanisms that drive repeat expansion disorders (Bellen et al., 2010).

2. Ease of Genetic Manipulation: The *Drosophila* system enables precise transgenic techniques, including the GAL4/UAS system, to express expanded trinucleotide repeats in a tissue-specific and inducible manner (Brand & Perrimon, 1993). For example, transgenic lines carrying expanded CGG or CAG repeats can be generated to mimic human neurodegenerative phenotypes, including protein aggregation and RNA foci formation.

3. Behavioral Assays: *Drosophila* displays complex behaviors, such as learning and memory, circadian rhythms, sleep, aggression, and motor activity—all of which can be quantitatively assessed. These behaviors

are frequently disrupted in disease models, offering direct readouts for neurological dysfunction (Guo, 2012; Sokolowski, 2001). For instance, locomotor assays are commonly used to model motor deficits seen in FXTAS and Huntington's disease.

4. Neurodegeneration Models: Repeat expansion models in *Drosophila* have successfully recapitulated neuronal loss, protein misfolding, mitochondrial dysfunction, and axonal degeneration, reflecting key hallmarks of neurodegenerative diseases (McGurk et al., 2015). These models help elucidate cell-type-specific vulnerability and can be used to test therapeutic candidates.

5. High-Throughput Screening Capability: Owing to its small size, short life cycle (~10 days), and ease of handling, *Drosophila* is amenable to large-scale genetic and pharmacological screening. These screens have been instrumental in identifying genetic modifiers and small molecules that mitigate neurotoxicity or aggregation phenotypes (Bonini & Fortini, 2003).

6. Experimental and Economic Advantages: The advantages of *Drosophila* include:

- Small body size and high fecundity
- Short generation time
- Low chromosome number and small genome (~165 Mb)
- Readily visible polytene chromosomes in salivary glands
- Cost-effective maintenance in laboratory settings

Moreover, *Drosophila* models not only recapitulate key molecular and behavioral phenotypes of repeat expansion disorders but also provide an efficient system for studying cell death, synaptic dysfunction, oxidative stress, and developmental dysregulation (Pandey & Nichols, 2011).

Overall, *Drosophila melanogaster* represents a valuable model organism that bridges the gap between in vitro studies and mammalian systems. Its use in repeat expansion disorder research continues to

provide deep insights into disease pathogenesis and offers a promising platform for preclinical drug discovery and the mechanistic dissection of genetic neurodegenerative diseases.

Chapter 2

Literature Review and Problem Formulation

Fragile X-associated Tremor/Ataxia Syndrome (FXTAS) is a late-onset neurodegenerative disorder caused by the abnormal expansion of CGG trinucleotide repeats (55–200) in the 5′ untranslated region (UTR) of the *FMR1* gene. Unlike Fragile X Syndrome, which results from full mutations (>200 repeats) and subsequent gene silencing, FXTAS arises in premutation carriers, where the gene is actively transcribed, but the RNA itself becomes pathogenic. The pathological hallmark of FXTAS includes the presence of intranuclear inclusions in neurons and astrocytes, along with brain atrophy, white matter lesions, and cerebellar degeneration (Hagerman & Hagerman, 2013).

FXTAS is predominantly observed in older male carriers, manifesting clinically as intention tremor, cerebellar ataxia, cognitive decline, Parkinsonism, and autonomic dysfunction. The disorder exhibits incomplete penetrance and variable expressivity, complicating both diagnosis and therapeutic development.

Molecular Pathogenesis

FXTAS pathogenesis involves two key molecular mechanisms:

1. RNA Toxic Gain-of-Function
   The expanded CGG repeat RNA forms stable noncanonical secondary structures—notably hairpins with GG 1×1 internal loops—that sequester several essential RNA-binding proteins such as DGCR8, Sam68, MBNL1, and hnRNP A2/B1. This sequestration impairs pre-mRNA splicing and miRNA processing, causing widespread transcriptional dysregulation and cellular stress (Sellier et al., 2010; Sofola et al., 2007).
2. Repeat-Associated Non-AUG (RAN) Translation
   In the absence of a canonical start codon, the CGG repeat undergoes RAN translation to generate toxic homopolymeric proteins, primarily polyglycine (FMRpolyG) and polyalanine (FMRpolyA), which

aggregates and disrupt neuronal homeostasis (Todd et al., 2013). These aggregates are detected in FXTAS patient brains and correlate with disease severity.

These dual toxic pathways—RNA-mediated protein sequestration and RAN translation-mediated proteinopathy—are central to FXTAS and present unique challenges for therapy development.

Therapeutic Landscape

To date, no FDA-approved therapies exist specifically for FXTAS. Current treatment strategies remain symptomatic, including beta-blockers and primidone for tremor, antidepressants for mood symptoms, and cognitive therapies. However, these interventions do not halt disease progression.

Given the RNA-based toxicity, a promising direction lies in targeting the expanded CGG RNA itself to either disrupt its abnormal structure or prevent protein sequestration and RAN translation.

Small Molecule Approaches

Several studies have identified small molecules that bind selectively to expanded CGG repeats. For instance:

- TMPyP4: A porphyrin derivative shown to bind CGG RNA and suppress RAN translation in FXTAS models (Krzyzosiak et al., 2012).
- A bisamidinium compound that binds CGG repeat RNA and prevents DGCR8 sequestration, rescuing miRNA processing (Park et al., 2021).
- Tilorone and Pentamidine: Initially used as antivirals or antimicrobials, these drugs have shown binding affinity to expanded repeats and reduce RNA foci in cellular models of FXTAS (Wang et al., 2020).

Despite this progress, none of these compounds are FDA-approved for FXTAS, and most remain in preclinical stages. Moreover, many face challenges such as poor CNS penetration, off-target interactions, and limited bioavailability, highlighting the need for alternative strategies.

Repurposing FDA-Approved Small Molecules

Given the success of small molecules in modulating RNA structures in disorders like Huntington's disease, repurposing FDA-approved drugs for FXTAS is a compelling strategy. These molecules often have favorable pharmacokinetic and safety profiles, and computational docking studies have revealed several that may bind CGG repeats with high affinity. For example:

- Zellou et al. (2022) demonstrated that certain kinase inhibitors and CNS-active drugs can disrupt CGG RNA foci formation.
- Myricetin, a natural flavonoid, has shown potential in reducing oxidative stress and modulating RNA structures in FXTAS models (Hashem et al., 2021).

The Way Forward

As with CAG repeat disorders, the pathogenesis of FXTAS is intricately tied to toxic RNA interactions, making RNA-targeting small molecules a central therapeutic focus. The future lies in identifying and optimizing such compounds, especially those already approved by the FDA for other indications, to fast-track clinical application.

This thesis will explore FDA-approved small molecules with the potential to bind and modulate CGG repeat-containing RNA, leveraging in silico, biophysical, and cellular assays. This work aims to bridge the gap between fundamental RNA biology and translational therapy for FXTAS and similar repeat expansion disorders.

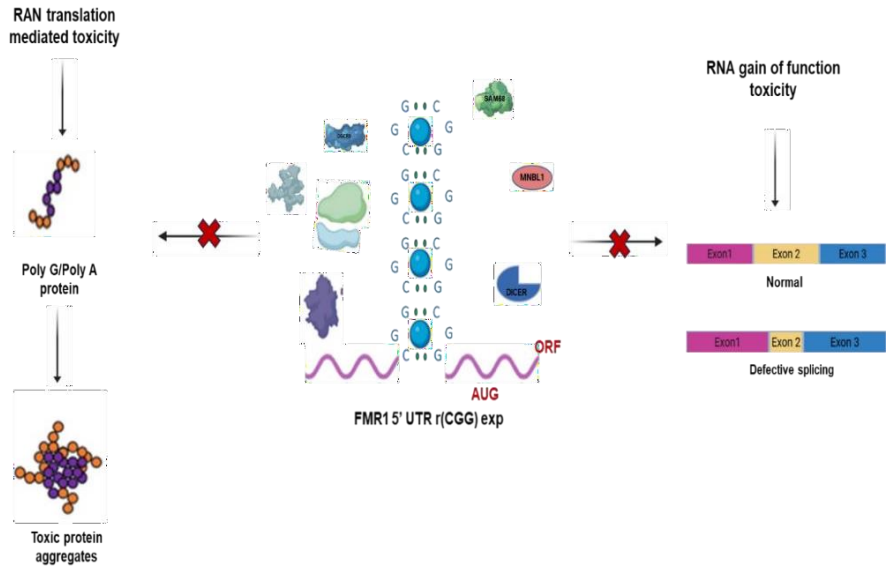

Figure 2.1: Schematic representation of potential therapeutics for FXTAS using small molecule drug targets.

Chapter 3

Materials, Methods, and Instrumentation

3.1 : Materials

The DNA oligonucleotides utilized in biophysical and molecular studies were acquired from Integrated DNA Technologies, located in Iowa, USA. Chemical substances such as NaCl, KCl, MgCl2, K2HPO4, KH2PO4, NaH2PO4, Na2HPO4, NaOH, HCl, Tris base, EDTA, DMSO, APS, TEMED, Acrylamide, Bis Acrylamide, ethanol, isopropanol, 2-butanol, methanol, urea, Triton-X 100, and others, were sourced from Sigma- Aldrich Chemicals Ltd., based in St. Louis, Missouri, USA and Sisco Research Laboratories Pvt. Ltd. in Mumbai, India. These were predominantly of HPLC-purified or molecular-grade quality. The dNTPs and rNTPs used for PCR and in vitro transcription reactions were also obtained from Sigma-Aldrich Chemicals Ltd. Additional materials such as Agarose, Luria broth, Luria agar, GC agar, and antibiotics like Ampicillin, Kanamycin, Chloramphenicol, Taq polymerase, and others were procured from Himedia Laboratories in India. Standard plasticware was supplied by Tarsons Products Pvt. Ltd. from Kolkata, India, while glassware was sourced from Borosil. The water purification system from Sartorius Corporate, Germany, was employed to produce molecular biology grade water essential for preparing buffers and media in various experiments.

3.2 : Sample preparation

3.2.1 : RNA oligo synthesis using T7 RNA Polymerase mediated in vitro transcription reaction.

3.2.1.1 : Expression and purification of T7 RNA Polymerase-

A single colony of transformed cells was cultivated in LB broth containing 50 μg/mL ampicillin and 34 μg/mL chloramphenicol and incubated overnight at 37 °C. For the secondary culture, fresh LB broth was inoculated, and the cells were grown with shaking at 37 °C until the OD600 reached 0.5. To induce protein expression, 0.5 mM IPTG

was added to the culture, and incubation continued for 4 hours at 37 °C. Post-induction, the cells were harvested by centrifugation at 9000 rpm, followed by a wash with lysis buffer.

Cell lysis was performed via sonication, using an amplitude of 55%, with cycles of 1 second on and 2 seconds off, for a total duration of 1 minute in the lysis buffer. The lysate was then centrifuged at 9500 rpm for 1 hour and 30 minutes at 4 °C. The supernatant was mixed with pre-cleaned, stripped, and recharged Ni-NTA beads and incubated with gentle agitation for 3-4 hours at 4 °C. This mixture was subsequently loaded onto an affinity chromatography column and washed with buffers in the following order: lysis buffer (4-5 column volumes), low-salt buffer (3-4 column volumes), and high-salt buffer (1-2 column volumes).

The target protein was eluted using lysis buffer supplemented with 300 mM imidazole and stored in storage buffer containing 100 mM NaCl, 50 mM Tris-HCl (pH 8.0), 10 mM DTT, and 50% glycerol at -20 °C for future use.

3.2.1.2：Polymerase chain reaction amplification

The template DNAs, as detailed in the appendix, were amplified using gene-specific forward and reverse primers with the help of Taq DNA Polymerase. The master mix, which included the primers, 4.25 mM MgCl2, 0.33 mM dNTPs, template DNA, and Taq DNA Polymerase, was aliquoted into individual PCR tubes.

The thermocycler was programmed to carry out the PCR, beginning with an initial denaturation at 95 °C. This was followed by 30 cycles, each consisting of denaturation at 92 °C for 30 seconds, annealing at the primer-specific temperature for 30 seconds, and extension at 72 °C for a duration proportional to the size of the target gene. A final extension step was performed at 72 °C for 10 minutes.

Following the PCR, the amplified products were examined using agarose gel electrophoresis and subsequently used for in-vitro transcription reactions.

3.2.1.3 *: In-vitro* transcription reaction

For all templates, a 25 μL transcription reaction was assembled at room temperature by sequentially adding: (i) 2.5 μL of 10× transcription buffer, (ii) 2 μL of 10× rTNP mix, (iii) 12.75 μL of template DNA, and (iv) 7.75 μL of T7 RNA Polymerase. The reaction mixture was incubated at 37 °C for 3-4 hours.

The transcription products were analyzed using 12% denaturing urea-PAGE gel electrophoresis. After electrophoresis, RNA bands were visualized by UV shadowing against a TLC plate. Bands corresponding to full-length transcripts were excised using a scalpel and transferred into tubes containing 300 mM NaCl. The gel slices were agitated overnight at 4 °C to extract RNA.

The tubes were centrifuged, and the supernatant was collected into new tubes. The RNA solution was washed twice with an equal volume of 1-butanol to remove impurities. RNA was then precipitated by adding chilled absolute ethanol, incubated at -80 °C for 2-3 hours, and centrifuged at 15600 rpm for 30 minutes at 4 °C. Residual ethanol was removed using rotary evaporation, and the RNA pellet was dissolved in molecular-grade water.

Desalting of the RNA was performed using a PD10 size-exclusion column. The eluted fractions were collected and lyophilized to obtain high-purity RNA.

3.3: Fluorescence Binding Assay

This study investigated changes in the fluorescence intensity of FDA-approved small molecules upon interaction with RNA. Fluorescence, a process where an electron transitions from an excited state to a lower energy state following excitation by high-energy electromagnetic radiation, emits visible light. The emitted energy depends on the

chemical environment of the electron, with the excitation and relaxation process occurring within approximately ten^{-8} seconds.

Unbound fluorophores typically exhibit minimal fluorescence due to their transient states. However, when bound to a macromolecule and undergoing conformational changes, fluorophores can produce significantly enhanced fluorescence or may transition to a photo-quenched state.

Fluorescence binding assays were performed at room temperature using Corning half-area black 96-well plates. Excitation and emission wavelengths specific to each molecule were determined in advance. To maintain uniformity, all wells contained an identical concentration of the small molecule. The assay was conducted in replicates to ensure accuracy. Ligands were first added to all wells, followed by a serial dilution of the RNA sample across wells up to the 11th, with the 12th well serving as a control without RNA. Fluorescence readings were recorded using a Synergy H1 multi-mode microplate reader. A binding equation for data fitting: both one mode and two mode data fits were used.

$$\boldsymbol{df} = \frac{\boldsymbol{Bmax1} * \boldsymbol{abs(x)}}{\boldsymbol{Kd1} * \boldsymbol{abs(x)}} + \frac{\boldsymbol{Bmax2} * \boldsymbol{abs(x)}}{\boldsymbol{Kd1} * \boldsymbol{abs(x)}}$$

Here, Bmax represents the maximum number of binding sites, and Kd denotes the equilibrium dissociation constant.

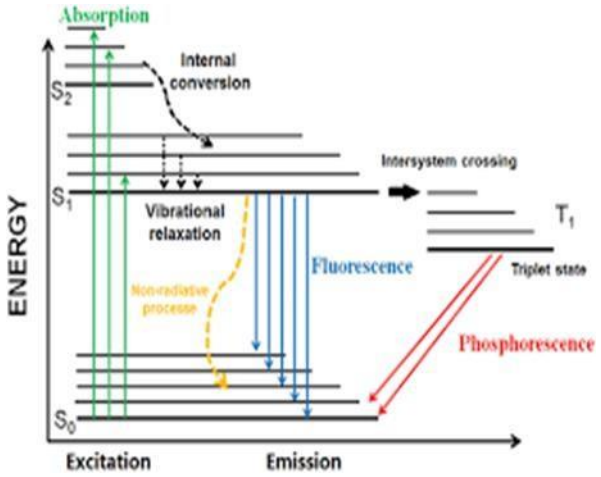

Figure 3.1: Jablonski's diagram of the fluorescence phenomenon

3.4: Circular Dichroism Spectroscopy

Circular Dichroism (CD) spectroscopy is a widely recognized analytical technique that measures the differential absorption of left and right circularly polarized light. This capability makes it invaluable for analyzing biological macromolecules' global structure and conformational dynamics in diverse chemical environments. The technique is particularly effective in identifying distinct conformational states of nucleic acids due to the asymmetric configuration of sugars in their backbone and the helical arrangement of nitrogenous bases. The differential absorption, known as CD, is represented mathematically as:

$$\mathbf{CD = A_l - A_r}$$

where $\mathbf{A_l}$ and $\mathbf{A_r}$ are the absorptions of left and right circularly polarized light, respectively. A CD spectropolarimeter consists of components that generate left and right circularly polarized light (LCP and RCP) and a photomultiplier (PMT) for detection. Biological macromolecules produce unique CD signals, known as signature CD spectra, which

correspond to specific conformational states. In nucleic acids, these signals result from chiral perturbations caused by glycosidic linkages between sugar units and nitrogenous bases. CD spectroscopy is particularly useful for analyzing the secondary structures of nucleic acids and their interactions with ligands or proteins. Variations in the position and intensity of CD spectral peaks reflect differences in topology and can also be influenced by the nucleic acid concentration.

In this study, CD titration experiments were conducted on in vitro synthesized RNA samples, with incremental additions of a lead small molecule. These measurements were performed at 25 °C using a scanning rate of 20 nm/min across the wavelength range of 190–300 nm. A Jasco J185 Spectropolarimeter was employed, and spectra were recorded in a 1 mm path-length cuvette. RNA concentrations were kept constant, while the small molecule concentrations were systematically varied. To ensure precise measurements, a blank spectrum of the buffer (1X KPO_4, KCl, and MQ water) was recorded prior to each sample measurement and subtracted from the RNA spectra. The resulting data were analyzed using SigmaPlot 13.0 to interpret ligand interactions and their effects on stabilizing or destabilizing loop structures.

Thermal profile assays were also carried out using CD spectroscopy. Thermal denaturation experiments were performed on a Perkin Elmer Lambda 35 spectrophotometer equipped with a Peltier temperature controller (PTP 6+6) and a water Peltier system PCB-1500. RNA samples were gradually heated from 25 °C to 95 °C at a rate of 1 °C per minute, while monitoring absorbance at 260 nm. These assays were conducted both in the absence and presence of the compound of interest, with varying D/N ratios. The data, showing normalized absorbance changes at 260 nm as a function of temperature, were plotted and analyzed using SigmaPlot 12.0 to derive insights into the compound's thermal stabilizing effects on the RNA structures.

3.5: CD melting

In this study, circular dichroism (CD) titration experiments were performed on in-vitro synthesized RNA samples, with incremental additions of a lead small molecule under controlled conditions at 25°C. The spectra were recorded using a Jasco J185 Spectropolarimeter at a scanning rate of 20 nm/min, covering a wavelength range of 190 to 300 nm. Measurements were taken in a cuvette with a 1 mm path length, maintaining a constant RNA concentration while varying the small molecule concentrations. To ensure accuracy, a blank spectrum of the buffer (1X KPO_4, KCl, MQ water) was recorded before each measurement and subtracted from the sample's CD spectrum. Data analysis was carried out using SigmaPlot 13.0, facilitating a comprehensive evaluation of ligand interactions and their impact on RNA loop structure stability.

Additionally, a thermal profile assay was conducted using CD spectroscopy. Thermal denaturation experiments were performed with a Perkin Elmer Lambda 35 spectrophotometer, equipped with a Peltier temperature programmer (PTP 6+6) and a PCB-1500 water Peltier system. RNA samples were gradually heated from 25°C to 95°C, while absorbance at 260 nm was monitored at a heating rate of 1°C per minute. These experiments were conducted both in the presence and absence of the test compound at varying D/N ratios. The resulting data, representing normalized absorbance changes at 260 nm as a function of temperature, were analyzed and plotted using SigmaPlot 12.0 software.

3.6: Electrophoretic mobility shift assay

The Electrophoretic Mobility Shift Assay (EMSA) is a rapid and susceptible technique used to determine the size and molecularity of biological macromolecules. It is beneficial for studying interactions between macromolecules. The principle of EMSA is based on the fact that the electrophoretic mobility of a molecule in a native polyacrylamide or agarose gel is influenced by factors such as its

charge, shape, and size. As a result, EMSA is commonly applied to investigate ligand-nucleic acid interactions, where the binding of a ligand to nucleic acid typically alters the molecular weight of the

nucleic acid, causing a shift in the mobility of the band during electrophoresis.

In this study, EMSA was performed using a 3% agarose gel in 1X TBE buffer. RNA samples were prepared in a 1X phosphate buffer containing 50 mM KCl and treated with varying concentrations of the lead drug molecule. These samples were incubated for 30 minutes at 25°C to allow the interaction to equilibrate.

Electrophoresis was carried out in a Bio-Rad Mini-Sub Cell GT Electrophoresis Cell. A total of 20 µl of each sample was loaded, and electrophoresis was run at room temperature with a voltage set at 72 V until the dye front moved three-fourths of the way down the gel. After electrophoresis, the gel was removed from the cassette and stained with Ethidium Bromide solution. The EMSA results were captured and analyzed using the ImageQuant LAS4000, an advanced imaging system from GE Healthcare Biosciences Ltd, Sweden.

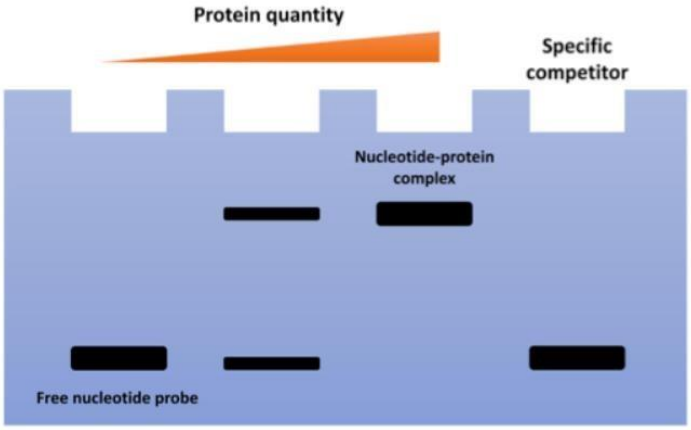

Figure 3.2: Schematic representation of Electrophoretic mobility shift assay.

3.7: PCR stop Assay

The template and complementary sequences used in this study were obtained from Sigma-Aldrich Chemicals Ltd., USA. The PCR stop assay master mix consisted of 1X PCR reaction buffer, 8 mM $MgCl_2$,

three µM oligonucleotides, one mM dNTPs, 2.5 units of Taq polymerase, and serial dilutions of the small molecule. The PCR protocol was as follows: an initial denaturation at 95°C for 3 minutes, followed by 30 cycles of 95°C for 30 seconds, 70°C for 30 seconds, and 72°C for 1 minute, with a final extension at 72°C for 10 minutes and then held at 4°C indefinitely. The PCR products were combined with 6X loading dye and separated on a 2.5% acrylamide gel without any added cations. The gel image was captured using the ImageQuant LAS 4000 system and analyzed with ImageJ software.

3.8: Nuclear Magnetic Resonance Spectroscopy

Nuclear Magnetic Resonance (NMR) spectroscopy is a fundamental analytical technique widely utilized in both chemical and biological research due to its exceptional ability to determine molecular structures, investigate dynamic processes, and analyze molecular interactions at the atomic level. The technique is based on the magnetic properties of atomic nuclei, particularly those with an odd number of protons or neutrons, which possess a magnetic moment. When placed in an external magnetic field (B_0), these nuclei align either parallel or antiparallel to the field. Upon exposure to radiofrequency (RF) pulses at a frequency corresponding to the energy gap between nuclear spin states, the nuclei undergo resonance, a phenomenon described by the Larmor equation:

$$\omega = \gamma B$$

where ω represents the angular frequency of the RF pulse, γ is the gyromagnetic ratio specific to each nucleus, and B denotes the applied magnetic field strength. The resonance process is highly sensitive to the surrounding chemical environment, leading to variations in the chemical shift, which provides crucial structural information

Additionally, interactions between nearby magnetic nuclei cause spin-spin coupling, observed as signal splitting in the NMR spectrum, offering insights into molecular connectivity.

An NMR spectrometer consists of several essential components designed to ensure precise measurements. A superconducting magnet generates a stable, high-intensity magnetic field, while RF transmitter and receiver coils facilitate the application of RF pulses and the

detection of emitted signals. The sample, typically dissolved in a solvent, is placed within a sample probe inside the magnetic field to ensure uniform exposure. Advanced pulse sequences, controlled by a dedicated system, manipulate nuclear spins to extract targeted information about the sample. The acquired data undergo processing using specialized software, enabling detailed spectral analysis.

NMR spectroscopy finds applications across diverse scientific fields. In chemistry, it plays a crucial role in determining the structures of organic molecules, analyzing complex mixtures, and monitoring reaction kinetics. In biological sciences, it is extensively used to study protein structures and dynamics, investigate ligand-receptor interactions, and explore metabolic pathways in metabolomics research. Additionally, in materials science, NMR helps characterize polymers, catalysts, nanoparticles, and other materials, providing valuable insights into their composition, structural properties, and functional attributes. With its non-destructive nature, high resolution, and ability to deliver in-depth structural data, NMR spectroscopy remains a cornerstone technique in research and innovation across multiple disciplines.

3.9 Assessing the Canonical GFP and Non-canonical FMR1 polyG-GFP Protein Aggregates

To ascertain the effect of P5 on FMR1 polyG-GFP aggregates, two different constructs of plasmids containing *r(CGG)x99-GFP* and *pcDNA-GFP* were used. Briefly, COS-7 cells were seeded in 12-well plates in 1X DMEM complete media. After the cell confluency

reached up to 80–90%, transfection was performed with the above-mentioned plasmid constructs using Lipofectamine 3000 reagents (purchased from Thermo Fisher Scientific) as per the manufacturer's standard protocol. Four hours following the transfection, the transfection cocktails were removed and replaced with media that contained P5. The peptides were added in a concentration-dependent manner, and the cells were incubated for 18–24 h at 37 °C with 5% CO_2. Following the treatment, the cells were washed with PBS and fixed with 4% paraformaldehyde for 15 min. The images were captured at high magnification using Fluorescence confocal microscopy to allow for detailed visualization of protein aggregates and processed to remove background signals. 100 positive transfected cells from each well were selected and manually counted with protein aggregates and

without protein aggregates from three different experiments. The number of GFP protein inclusions was also manually counted from three independent experiments, and standard deviations were calculated.

3.10 : Quantification of RAN Translation by Western blot

HEK293 cells were cultured in a 6-well plate in a monolayer and transfected with 2.5 µg of a plasmid encoding CGGx99-GFP using Lipofectamine 3000, following the manufacturer's protocol from Thermo Fisher Scientific. After 5 hours of incubation, the transfection mixture was replaced with fresh media containing the compound, and the cells were incubated for an additional 24 hours at 37°C. Following incubation, cells were lysed with 200 µL/well of RIPA buffer containing 1 µL of Halt Protease Inhibitor Cocktail from Sigma. The protein concentration was determined using the Bradford assay. Equal amounts of protein were loaded onto an SDS-PAGE gel for separation and then transferred to a PVDF membrane. The membrane was incubated with an anti-FMR1-polyG antibody (Merck Millipore) as the primary antibody. After primary antibody incubation, an anti-IgG-HRP conjugate was used as the secondary antibody. Chemiluminescent

signals were detected using the Luminata Crescendo Western HRP substrate (Merck Millipore) on an ImageQuant LAS 4000 system (GE Healthcare).

3.11 : Improvement in splicing defects in the FXTAS cellular model

To evaluate whether the selected molecule enhances alternative splicing defects in vitro, an FXTAS cellular model was utilized. HEK293 cells were cultured in 24-well plates in a monolayer with growth medium consisting of 1X DMEM, 10% fetal bovine serum, and 1% antibiotic-antimycotic solution at 37°C with 5% CO2. Once the cells reached 80-90% confluency, they were transfected with an equal amount of plasmid containing the CGGx99 repeat and the targeted mini-gene (SMN2) using Lipofectamine 3000 reagent (Thermo Fisher Scientific) following the manufacturer's protocol. After 4-5 hours, the

transfection mixture was replaced with DMEM containing Curcumin, and the cells were incubated for an additional 24 hours. Following incubation, the cells were lysed, and total RNA was extracted using an RNA isolation kit (Invitrogen) as per the manufacturer's guidelines.

The extracted RNA samples were reverse transcribed using a cDNA synthesis kit from Bio-Rad, following the standard protocol. Of the 500 ng of reverse-transcribed mRNA, 100 ng was used for semi-quantitative PCR. The PCR conditions included denaturation at 95°C for 1 minute, annealing at 55°C for 1 minute, extension at 72°C for 2 minutes, and a final extension at 72°C for 10 minutes, with 25-30 cycles. The PCR products were analyzed via agarose gel electrophoresis, stained with ethidium bromide, and the images were captured using the ImageQuant LAS 4000 system (GE Healthcare). Splicing isoform intensity was quantified using ImageJ software. Primer sequences for each construct are provided in Table S4.

Two control conditions were applied to examine pre-mRNA splicing defects: (1) co-transfection of the targeted mini-gene (SMN2) with a plasmid lacking the CGG repeat in the 5' UTR, and (2) co-transfection

of the CGG repeat plasmid with mini-genes whose pre-mRNA splicing is not regulated by Sam68 (cTNT).

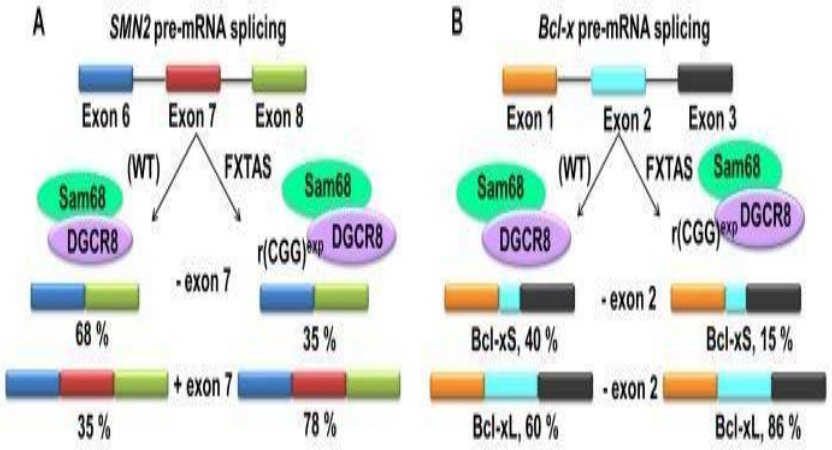

Figure 3.3: Schematic representation of the occurrence of splicing defects in FXTAS

3.12 : MitoSOX™ Red Staining in COS-7 Cells

MitoSOX™ Red mitochondrial superoxide indicator was used to detect and quantify mitochondrial superoxide production—a major contributor to oxidative stress—in the context of neurodegenerative disease modeling. In many neurodegenerative disorders, such as Huntington's disease, Alzheimer's disease, Parkinson's disease, and Fragile X-associated Tremor/Ataxia Syndrome (FXTAS), mitochondrial dysfunction and elevated reactive oxygen species (ROS), particularly mitochondrial superoxide, are strongly implicated in disease progression and neuronal toxicity. Assessing mitochondrial ROS levels provides insight into the cellular stress and damage mechanisms triggered by pathological mutations or toxic protein aggregates.

COS-7 cells were cultured in Dulbecco's Modified Eagle Medium (DMEM) supplemented with 10% fetal bovine serum (FBS) and 1% penicillin-streptomycin, and plated on poly-D-lysine-coated glass coverslips in a 24-well plate at a density of 1×10^5 cells/well. After

cells reached approximately 70% confluency, they were subjected to the relevant experimental treatments, such as transfection with plasmids expressing toxic RNA or protein species associated with repeat expansion disorders.

Following treatment, cells were washed twice with warm Hank's Balanced Salt Solution (HBSS) without phenol red. A working solution of MitoSOX™ Red reagent (Thermo Fisher Scientific, M36008) was freshly prepared at a final concentration of 5 μM in HBSS. Cells were incubated with the staining solution for 10 minutes at 37°C in the dark to allow mitochondrial uptake of the dye and specific reaction with superoxide. After incubation, cells were washed three times with HBSS to remove excess dye.

Coverslips were mounted using an antifade mounting medium, and fluorescence imaging was performed immediately using a fluorescence microscope equipped with the appropriate filter set (excitation/emission: 510/580 nm). Images were analyzed using ImageJ to quantify mean fluorescence intensity per cell as a measure of mitochondrial oxidative stress. The experiment was performed in biological triplicates, and representative fields were imaged for consistency. This approach enables the evaluation of mitochondrial ROS generation in response to neurodegenerative disease-related stressors and the efficacy of antioxidant or therapeutic interventions.

3.13 : TMRM Staining in COS-7 Cells

Tetramethylrhodamine methyl ester (TMRM) staining was performed to assess mitochondrial membrane potential (Δψm), a key indicator of mitochondrial health and function. Mitochondrial membrane potential is often disrupted in neurodegenerative disorders such as Huntington's disease, Parkinson's disease, and Fragile X-associated Tremor/Ataxia Syndrome (FXTAS), where toxic protein or RNA aggregates impair mitochondrial dynamics and bioenergetics. Monitoring Δψm using TMRM provides valuable insights into early mitochondrial dysfunction, a hallmark of neuronal degeneration.

COS-7 cells were cultured in complete DMEM supplemented with 10% fetal bovine serum (FBS) and 1% penicillin-streptomycin and seeded onto poly-D-lysine-coated glass coverslips in a 24-well plate at a density of 1×10^5 cells/well. After achieving 70–80% confluency, cells were subjected to the experimental conditions, such as transfection with constructs expressing disease-associated repeat expansions or mutant proteins.

Following treatment, cells were washed twice with warm phosphate-buffered saline (PBS), and a working solution of TMRM (Thermo Fisher Scientific, T668) was prepared at a final concentration of 50 nM in serum-free, phenol red-free DMEM. Cells were incubated with the TMRM solution for 30 minutes at 37°C in a CO_2 incubator, protected from light. This dye accumulates in active mitochondria in proportion to the membrane potential due to its positive charge. After staining, cells were washed gently with PBS and immediately imaged live using a fluorescence microscope equipped with a TRITC filter set (excitation/emission: ~548/573 nm). Mean fluorescence intensity per cell was measured using ImageJ software to assess changes in mitochondrial membrane potential. A decrease in TMRM fluorescence indicates mitochondrial depolarization, reflective of impaired mitochondrial function. The assay was repeated in triplicate, with at least five random fields analyzed per condition. This method allows for the sensitive detection of early mitochondrial dysfunction, which is crucial in understanding and potentially intervening in the pathogenesis of neurodegenerative disorders.

3.14 : *Drosophila* fly stocks, food, and their maintenance

Flies were reared on standard cornmeal-agar (HiMedia Drosophila Diet) supplemented with antibiotic and propionic acid, with a 12-hour on–off light cycle at 25 °C.

The following fly stocks have been used:

1) UAS-Httex1Q20 (non-pathogenic): Expresses human HTT exon 1 with 20 CAG repeats under the control of UAS.

2) UAS-Httex1Q93 (pathogenic): Expresses human HTT exon 1 with 93 CAG repeats under the control of UAS.

3) GMR-Gal4: A Gal-4 stock that expresses GMR (Glass Multiple Reporter) in all cells posterior to the morphogenetic furrow, and later it becomes active throughout most of the pupal eye.

4) Elav-Gal4c155 driver line: The "Elav-Gal4" driver line in Drosophila melanogaster drives expressionof genes specifically in neurons when combined with Gal4-responsive promoters.

Males of all the transgenic lines used in the study were crossed with virgins of elav-Gal4 and GMR-Gal4 to drive their expression in the fly brain and the eye-imaginal discs, respectively. The flies were maintained on a typical cornmeal-agar diet at a temperature of 25±1°C

with consistent light-dark cycles and humidity ranging from 70% to 80%. Drug of choice was added to the fly food at concentrations of 10 μM, 25 μM, and 50 μM to rear experimental larvae or flies. Control groups were raised on regular food without the drug at a temperature of 25°C.

3.15 : Rough eye phenotype assessment

The rough eye phenotype of flies expressing Httex1p Q93 under the control of gmr-GAL4 was evaluated. These flies were cultured at 25 °C on standard food and food supplemented with either 5, 10, or 25 mM drug compound. The outer surface of the fly eye was scrutinized using a Nikon SMZ745T microscope on days 1, 7, and 14 after emergence. A total of 30 flies were examined for each condition.

3.16 : Scanning Electron Microscopy Images for *Drosophila* external eye.

The Critical Point Dried (CPD) method was used to prepare samples for attaining high-magnification analysis through Scanning electron microscopy as per Kimmel et al. (1990). First, whole flies were immersed in a fixative composed of (1% glutaraldehyde, 1% formaldehyde, and 1M sodium cacodylate (pH 7.2)) for 2 hours.

Further, to submerge the flies in the fixative, single drops of 0.2% Tween 20 (diluted in H20) were used. This was followed by rinsing in H20. Then, the flies were dehydrated in an Ethanol series (once in 25%, 50%, and 75% ethanol and twice in 100% ethanol), each for 12 hours, at room temperature. The flies were then fixed, and images were taken, followed by CPD and sputter-coating.

3.17 : Negative geotaxis

The negative geotaxis assay was employed to assess age- and condition-dependent changes in the locomotor capabilities of *Drosophila melanogaster*, which are indicative of neuromuscular function and general motor coordination. This innate behavior, where flies move upward against gravity following a mechanical disturbance,

was utilized as a quantitative and reproducible readout for climbing ability.

Flies from each experimental condition were tested in two independent biological replicates, with each replicate consisting of 10 adult flies (3–5 days old), maintained under identical conditions. Prior to testing, flies were transferred into clean, transparent acrylic assay tubes measuring 25 cm in height and 1.5 cm in inner diameter, and allowed to acclimate for 15 minutes at room temperature to reduce stress-induced variability. The interior of each tube was marked at a height of 8 cm from the base to serve as the scoring threshold.

For the assay, flies were gently tapped down to the bottom of the tube three consecutive times to initiate the climbing response. Immediately after tapping, a stopwatch was started, and the number of flies that successfully climbed past the 8 cm mark within 20 seconds was recorded. This procedure was repeated across six consecutive trials for each condition, with a 1-minute rest period between each trial to avoid fatigue effects. To minimize potential bias, all trials were conducted at a consistent time of day under ambient light conditions.

Performance was quantified as the percentage of flies that crossed the threshold distance during each trial. The average success rate across trials was calculated and used for statistical comparison between control and treated groups. The assay provided insights into the effects of genetic modifications, aging, or pharmacological treatments on motor function in *Drosophila*.

3.18 : Crawling Assay

The larval crawling assay was employed to assess the neuromuscular coordination and locomotor abilities of third-instar *Drosophila melanogaster* larvae under different experimental conditions. The assay was conducted using a standard round petri dish (100 mm × 10 mm) filled with a 3.3% agar solution, which provided a semi-solid, moist surface ideal for facilitating larval movement while preventing desiccation or slippage.

A narrow track was carefully carved into the surface of the agar using a sterile blade. The track measured approximately 2 mm in width, 30 mm in length, and 5 mm in depth, providing a defined corridor that limited lateral movement and ensured consistent locomotion measurements across all trials. The temperature and humidity of the testing environment were kept constant to minimize behavioral variation due to environmental factors.

For each experimental group, ten healthy third-instar larvae were individually placed at the starting point of the track using a fine brush. Larvae were allowed to acclimatize for a few seconds before observation. The movement of each larva along the track was recorded over a 20-second interval using a high-resolution camera mounted above the dish. Crawling was defined as the coordinated forward movement of the entire body, measured either by the total distance traveled within the time frame or by counting the number of peristaltic waves.

Two independent trials were conducted for each condition to ensure reproducibility and minimize observer bias. Crawling data were

analyzed using ImageJ or similar motion-tracking software, and the average speed (mm/sec) or distance traveled was calculated for each larva. Results were then statistically compared between control and treatment groups to assess the impact of genetic manipulations or pharmacological interventions on larval locomotion.

3.19 : Flight assay

The flight assay was conducted to evaluate the aerial locomotor ability of *Drosophila melanogaster* under different experimental conditions. A vertical Plexiglas flight column measuring 100 cm in height and 10 cm in diameter was used for this purpose. The inner wall of the column was coated with a thin layer of mineral oil or lined with transparent adhesive film to capture the landing positions of the flies after their descent. The column was divided into five equal horizontal zones, each 20 cm in height, to facilitate quantification of flight performance.

For each condition, two independent groups comprising 20 adult flies (3–5 days old) were selected and briefly anesthetized on ice to reduce handling stress. Flies were carefully transferred into a small funnel positioned at the top of the column and were allowed to recover for a minute before release. Upon release, flies initiated flight spontaneously and either actively flew or passively dropped within the column. After a fixed duration of 10–15 seconds, the position at which each fly adhered to the wall was recorded. Flies that were capable of initiating flight tended to land in the upper or middle zones, while those with impaired flight ability accumulated in the lower zones or directly at the bottom.

Each assay was repeated three times to ensure reproducibility and to minimize variability due to handling or recovery time. The data were analyzed by calculating the percentage of flies in each of the five zones, and a weighted flight index was computed to provide an aggregate measure of flight

proficiency. This index allowed for statistical comparison between control and experimental groups, aiding in the evaluation of phenotypes resulting from genetic manipulation or drug treatment.

3.20 : Quantification of RAN Translation by Western blot in *Drosophila* FXTAS model.

To extract total protein from *Drosophila melanogaster*, adult flies were first anesthetized on ice and collected in 1.5 mL microcentrifuge tubes. For each experimental condition, approximately 20–30 adult flies were pooled to ensure sufficient protein yield. The flies were rapidly flash-frozen in liquid nitrogen and stored at –80°C until use. Frozen flies were homogenized using a motorized pestle in 200–300 µL of ice-cold CytoEB1X buffer. Homogenization was carried out thoroughly on ice to ensure complete tissue disruption. After homogenization, the lysates were incubated on ice for 20 minutes to allow complete lysis, followed by centrifugation at 13,000 × g for 15 minutes at 4°C. The supernatant, containing the soluble protein fraction, was carefully collected into

fresh microcentrifuge tubes, while the pellet containing debris was discarded.

The protein concentration was determined using the Bradford assay. Equal amounts of protein were loaded onto an SDS-PAGE gel for separation and then transferred to a PVDF membrane. The membrane was incubated with an anti-FMR1-polyG antibody (Merck Millipore) as the primary antibody. After primary antibody incubation, an anti-IgG-HRP conjugate was used as the secondary antibody. Chemiluminescent signals were detected using the Luminata Crescendo Western HRP substrate (Merck Millipore) on an ImageQuant LAS 4000 system (GE Healthcare).

Chapter 4

Results and discussion

To assess how well several FDA-approved small molecules target and interact with r(CAG)exp, we conducted a range of biophysical experiments to determine their specificity and selectivity in reducing the toxic effects of Poly-Q proteins.

4.1: Fluorescent binding assay

Fluorescent binding assay was performed with a library of 14 drugs from P1 to P14, against (CGG)6 repeat RNA. The bar graph below shows the value of dissociation constant (Kd) for all 14 drugs with (CGG)6 repeat RNA. The value of Kd is inversely related to the binding affinity. Thus, the molecule P5 with lesser Kd value was chosen for the study. This was a primary screening step used to select the molecule that shows specific binding to target repeat RNA. The result for this screening is shown below.

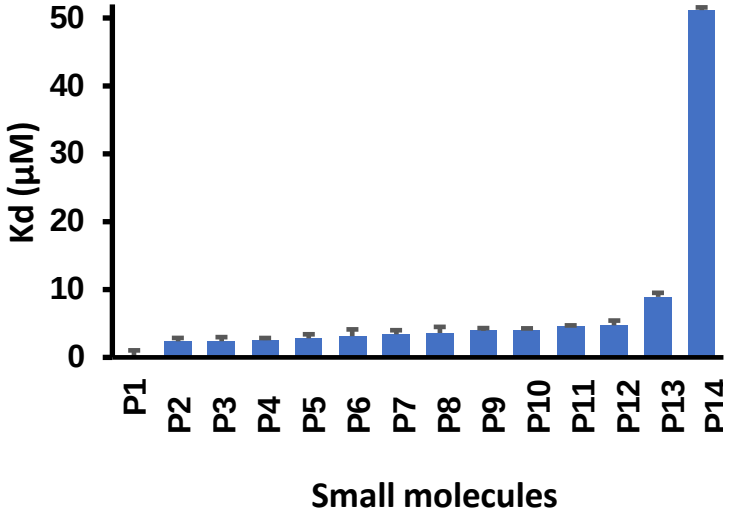

Figure 4.1: Bar graph representing Kd values of the library of 14 small molecule with (CGG)6 repeat RNA.

Based on this primary screening molecule P5 was selected to further analyse the selective binding abilities with target repeat RNA. The PubChem structure molecule P5 is shown.

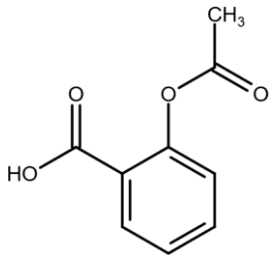

Figure 4.2: PubChem structure of P5

The excitation wavelength of the molecule P5 is 290nm, and the emission wavelength is 310nm. Further fluorescence binding assays were performed with the library of 11 RNA sequences containing 1 × 1 internal loop motifs. RNA 5'CAG/3'CUG is used as a control RNA because it does not contain any mismatch because of A-U canonical matching, and thus, change in the fluorescence intensity after incubation of FDA-approved small molecules would indicate binding with control and thus would not be considered for further experimentation. The results for these binding assays are as follows

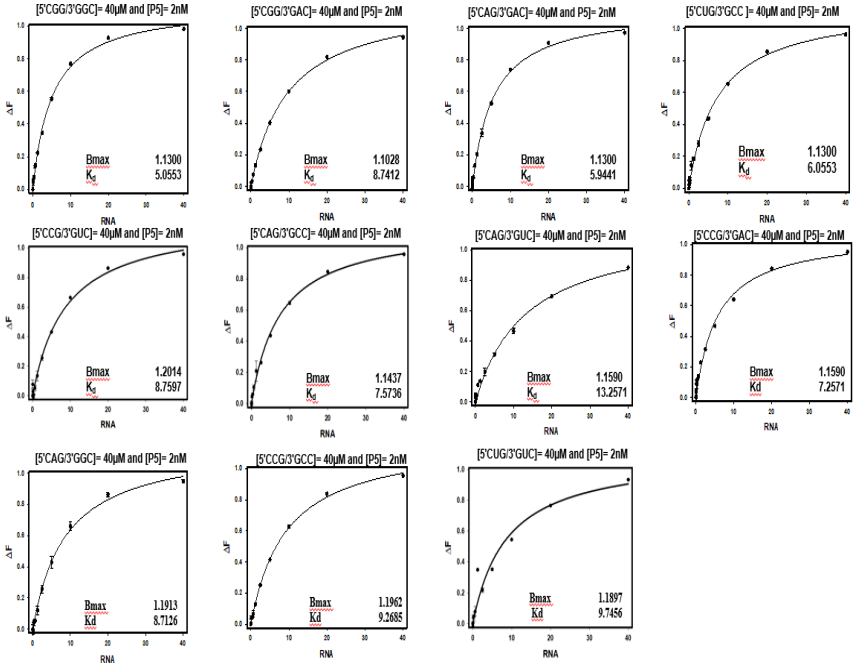

Figure 4.3: Plots of fluorescence titration of P5 with 11 RNA sequences with 1x1 internal RNA motif

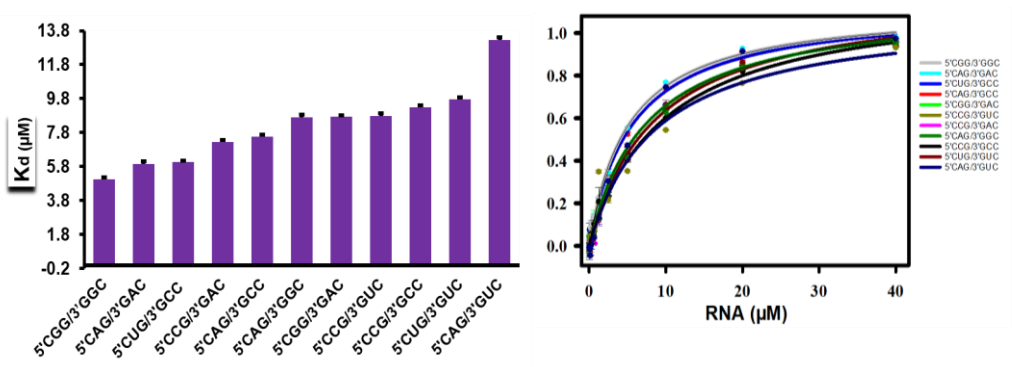

Figure 4.4: Evaluation of molecule P5 using fluorescence binding assay. The bar graph denotes the k_d of 11 RNA sequences containing 1x1 internal loop with P5. The plot represents the fluorescence titration assay one-mode curve fitting of 11 RNA sequences containing 1x1 internal loop with P5.

The results showed the lowest value of Kd with the target loop (5'CGG/3'GGC), whereas the control loop (5'CAG/3'GUC),

indicating the selective binding efficiency of P5 with target repeat RNA.

Further fluorescence binding assays with different length expanded (CGG) repeats were performed. The result for these binding assays is as follows.

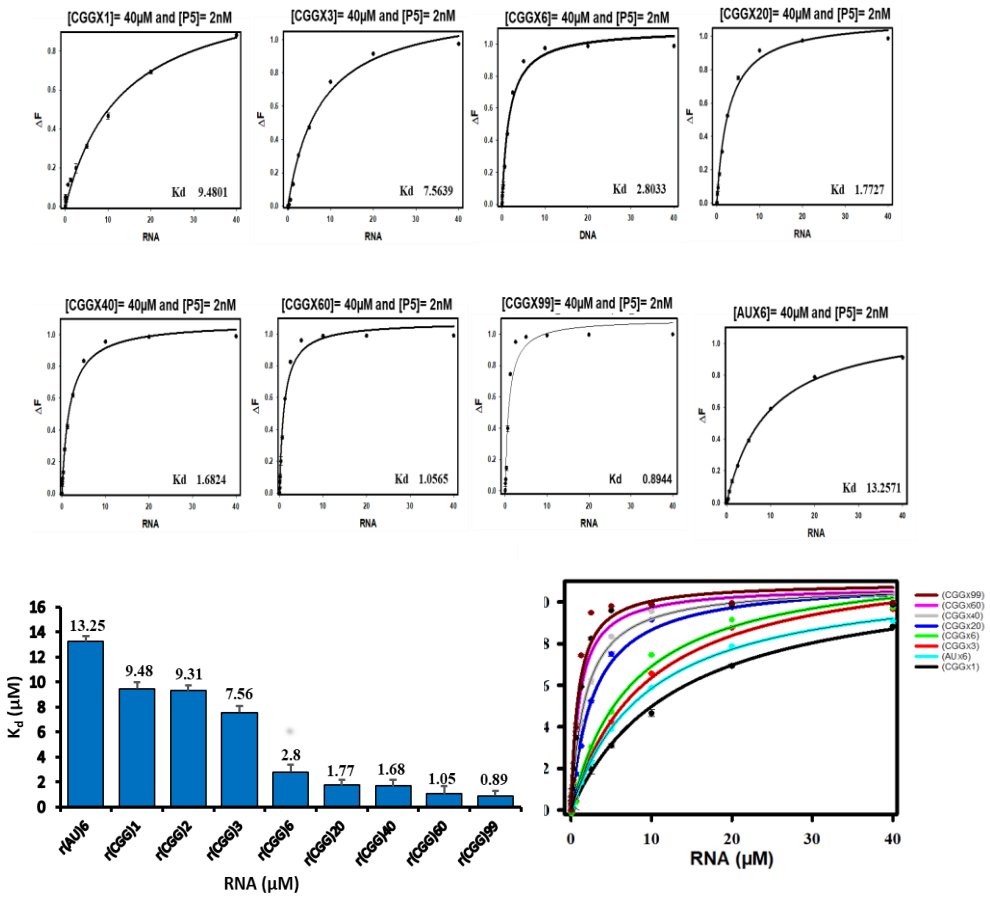

Figure 4.5: Evaluation of molecule P5 using fluorescence binding assay. The bar graph denotes the k_d of of extended r(CGG) RNA with P5. The plot represents the fluorescence titration assay one-mode curve fitting of extended r(CGG) RNA with P5.

The results showed a gradual decrease in the value of Kd with increasing length of expanded repeats, showing that the binding is

further enhanced upon increasing the repeat length. (AU)6 RNA was taken as control.

Further binding assays were performed with various DNA/RNA controls to eliminate the dilemma of non-specific binding of small molecules. The results are as follows

The results obtained showed that the Kd values for all the control DNAs/RNAs were significantly higher than that of target RNA repeat, which eliminates the parameter of non-specific binding of small molecule

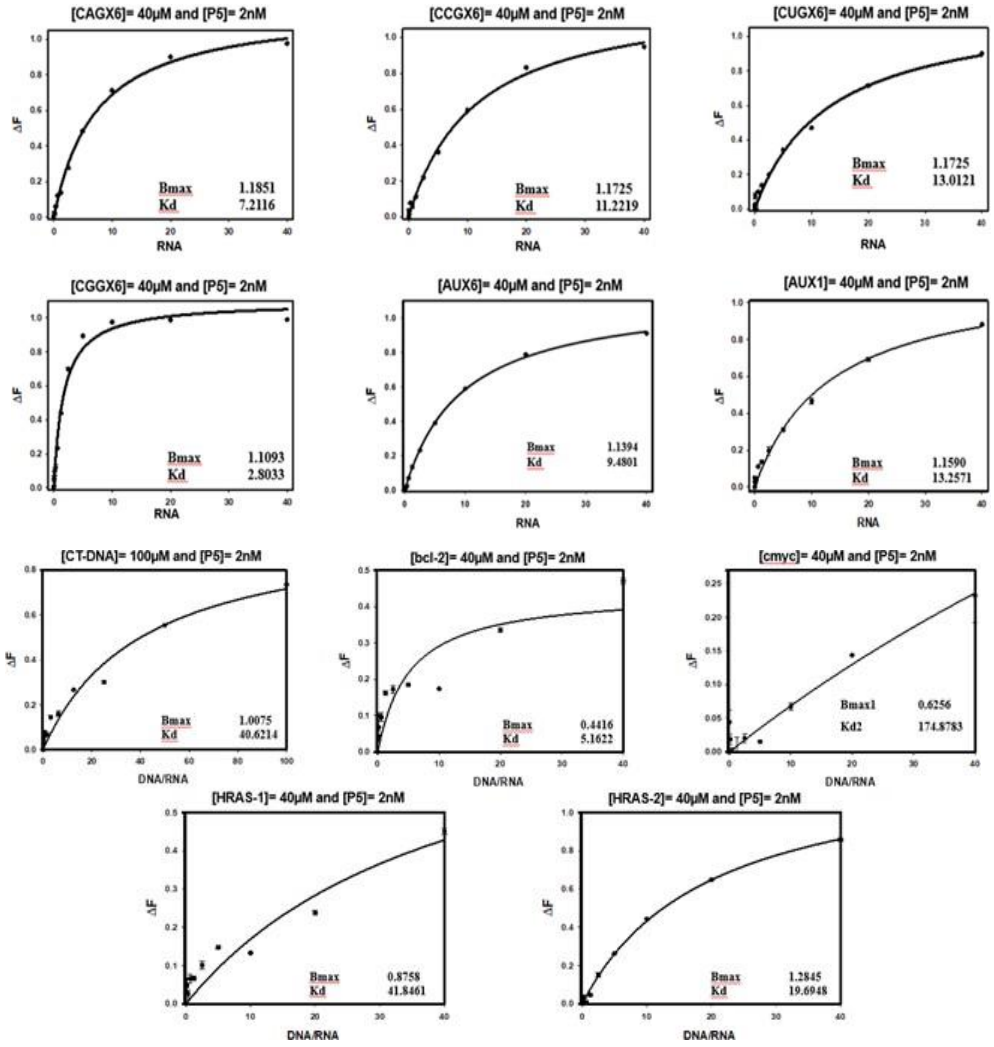

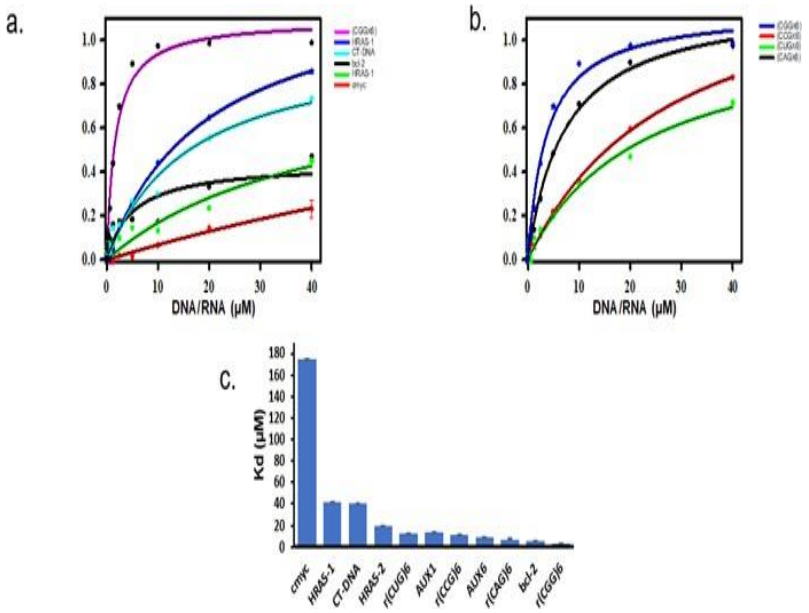

Figure 4.6: Plots of fluorescence titration of P5 with different DNA/RNA control

4.2 Circular Dichroism Spectroscopy

A positive band around 265–270 nm and a negative band around 215–220 nm typically characterize the CD spectrum of CGG repeat RNA, which is similar to A-type RNA confirmation. The gradual addition of P5 to CGG repeat RNA caused a major hypochromic shift and red shift in the negative peak, whereas the overall RNA structure was found to remain the same. The CD titration of P5 with other r(CNG)^{exp} and r(AU) duplex RNAs also affirms the selectivity of P5 for CGG repeat RNA.

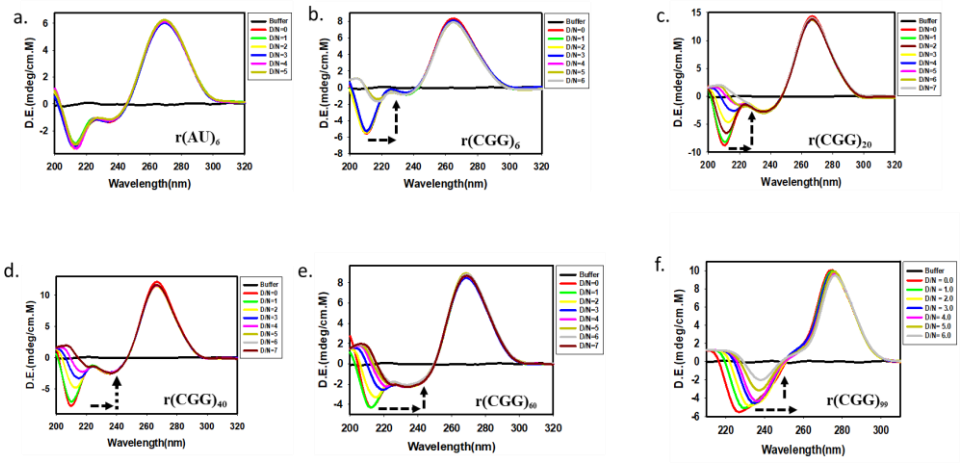

Figure 4.7. Circular dichroism spectroscopy titration of r(CGG)^{exp} and r(AU)^{exp} duplex RNAs in the presence of P5. (a) r(AU)$_6$, (b.)r(CGG)$_6$, (c.) r(CGG)$_{20}$, (d.) r(CGG)$_{40}$, (e.) r(CGG)$_{60}$, and (f.) r(CGG)$_{99}$ RNA. In the presence of P5, significant spectroscopic changes were detected with CGG repeat RNAs compared to other mismatched RNA motifs and AU duplex RNAs. D/N denotes the drug-to-nucleotide ratio.

4.3: CD Melting analysis

CGG RNA thermal profiles were monitored at 267 nm, and significant changes in melting temperature (ΔT_m) were observed for r(CGGx20), r(CGGx40), and r(CGGx60). In contrast, no change in melting temperature was found as a function of P5 concentration with AU pair duplex RNA. Interestingly, large changes in melting temperature were found in RNAs with higher repeat numbers as compared to lower repeat RNAs. In conclusion, P5 enhances the thermal stability of all tested CGG-targeted RNAs, indicating that P5 stabilizes the CGG RNA structure, which may prevent ribosomal assembly to initiate RAN translation and/or interaction of the RNA-binding proteins that mediate FXTAS-splicing defects.

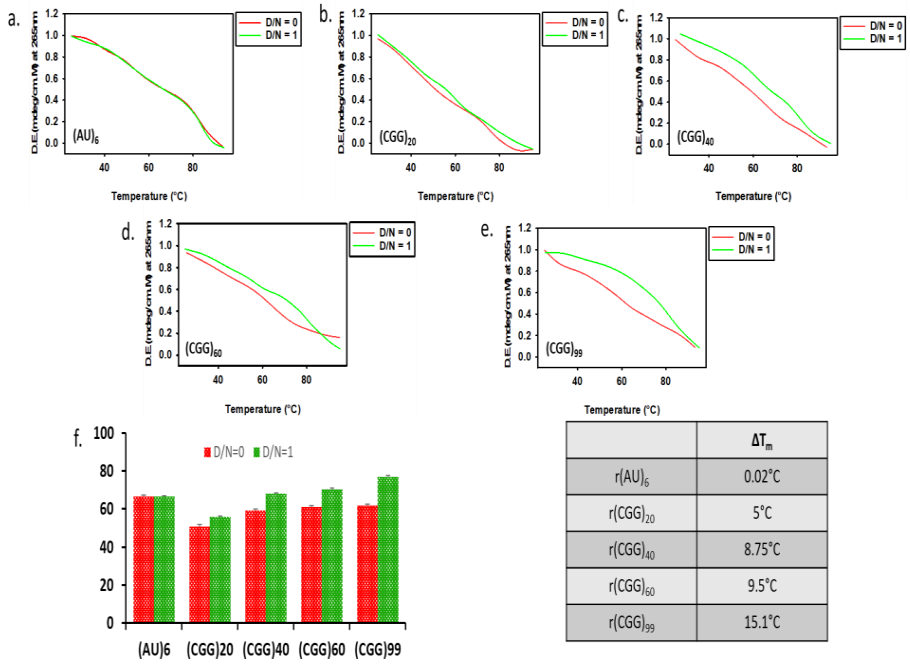

	ΔT_m
$r(AU)_6$	0.02°C
$r(CGG)_{20}$	5°C
$r(CGG)_{40}$	8.75°C
$r(CGG)_{60}$	9.5°C
$r(CGG)_{99}$	15.1°C

Figure 4.8: A systemic representation of the thermal denaturation profile of $r(CGG)_{exp}$ RNAs with P5. (a.) $r(AU)_6$, (b.) $r(CGG)_{20}$, (c.) $r(CGG)_{40}$, (d.) $r(CGG)_{60}$, and (e.) $r(CGG)_{99}$ RNAs with P5. (f.) The bar graph shows the ΔT_m values of the expanded CGG repeats RNAs with P5.

4.4: Electrophoretic mobility shift assay

On increasing the concentration of P5, the retardation in the migration of the band was observed in $r(CGG)^{exp}$ RNAs. The shift in the mobility was due to the sequence and motif-specific interactions that allow the formation of a stable complex between P5 and $r(CGG)^{exp}$ RNAs. Furthermore, we also found that higher repeats of CGG RNA, $r(CGG)_{40}$ and $r(CGG)_{60}$, showed prominent retardation in the migration. In contrast to CGG RNA, other mismatched RNA motifs and AU-paired duplex RNA showed no such significant retardation.

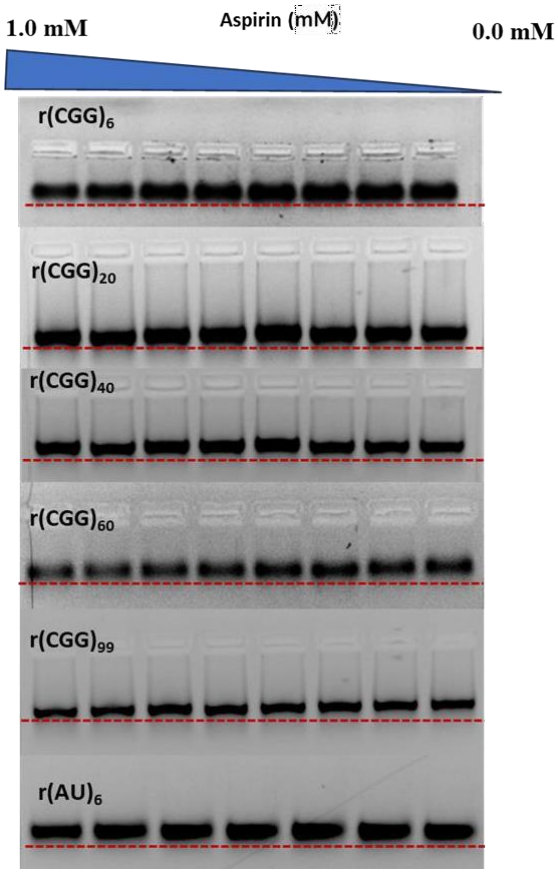

Figure 4.9: Gel retardation assay. The gel images shows that an increasing concentration of P5 significantly retards the mobility of CGG repeat RNAs over AU duplex RNA

4.5: PCR stop assay

Furthermore, we also performed the polymerase chain reaction (PCR) stop assay to elucidate further the binding affinity of P5 with CGG repeat sequences using DNA templates. P5 binds to the CGG repeat motif and impairs the polymerase activity during extension. Similar to the gel retardation assay, with the gradual addition of P5 the intensity of PCR bands decreased, suggesting the arrest of polymerase enzyme movement during extension. On the other hand, no significant changes were observed in the intensity of the PCR product of other mismatch and AU pair DNA. These observations effectively characterize P5 as a CGG-interactive compound that stabilizes the CGG repeat RNA hairpin structure.

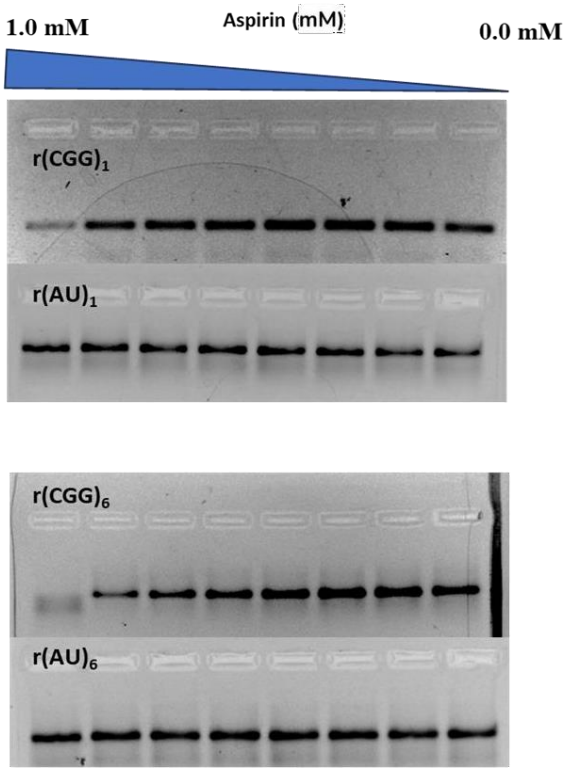

Figure 4.10: PCR stop assay. Gel images show the decreased intensity of PCR product with increasing concentration of P5 compared with AU paired template.

4.6: NMR Spectroscopy

Following the assessment of the binding affinity of the peptides and the $r(CGG)_{exp}$, our next objective was to elucidate the atomic-level intricacies of these interactions. Thus, we carried out an NMR titration assay of $r(CGG)_6$ with P5. The alterations in the resonance peak amplitude, broadening, and chemical shift of protons were systematically observed throughout each stage of the titration process. The results showed the involvement of protons of P5 with $r(CGG)_6$ RNA.

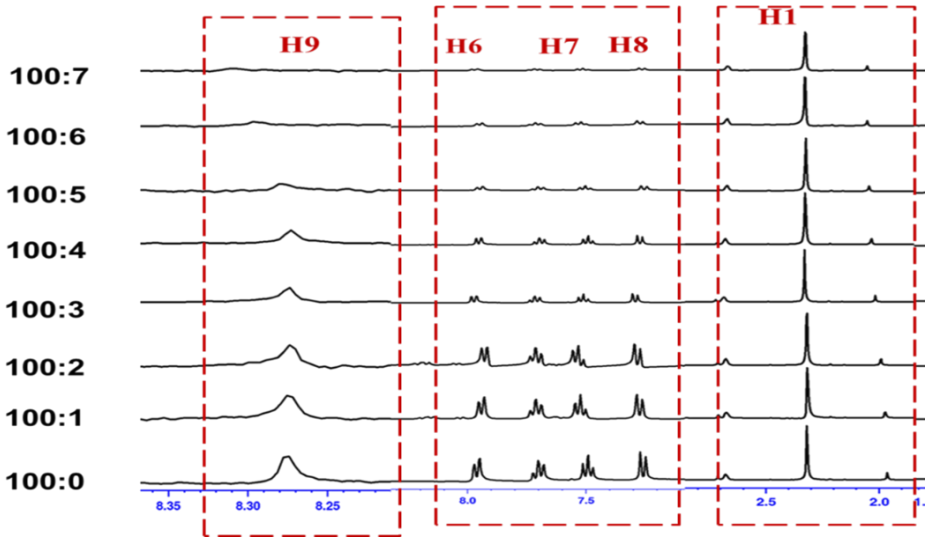

Figure 4.11: Represents NMR peak broadening upon titration of P5 with $(CGG)_6$ RNA.

4.7: Assessing the Canonical GFP and Non-canonical FMR1 Poly G-GFP Protein Aggregates

Fluorescence images show a decrease in Poly-G aggregates with increasing concentration.

Fluorescence microscopy images show a decrease in aggreated from 100 percent in control condition to around 20 percent in drug treated cellular model at a concentration of 50.0 µM. The line graph depicts the same result.

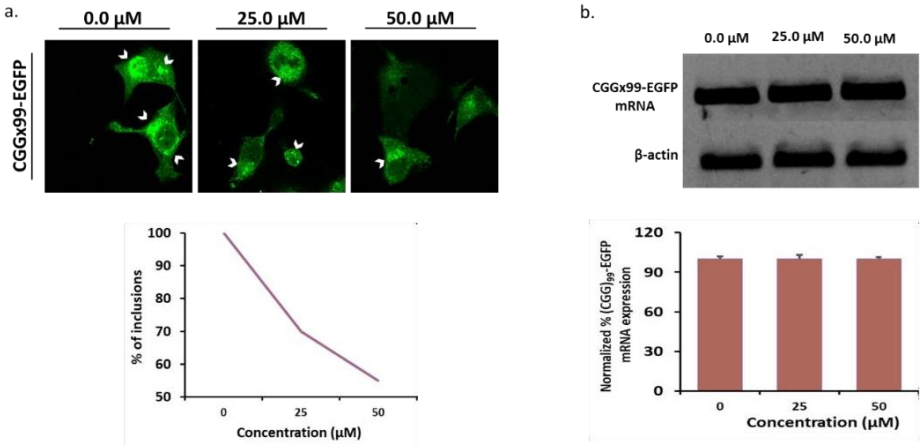

Figure 4.12: (a.) Images represent the FMR1polyG-GFP inclusions in r(CGG)x99-EGFP expressing COS7 cells with P5 at different concentrations. The accompanying line graph represents the percentage reduction of inclusion numbers post-treatment with P5. (b.) Gel image shows CGGx99-EGFP mRNA expression. The accompanying bar graph represents the percentage normalized $(CGG)_{99}$-EGFP mRNA expression post-treatment with P5.

4.8: Quantification of RAN Translation by Western blot

After assessing the affinity and selectivity of P5 to $r(CGG)^{exp}$ motifs containing target RNA, we further sought to determine the ability of P5 to reduce cellular toxicity caused by $r(CGG)^{exp}$ RNA in the FXTAS cellular models. To develop an FXTAS cellular model, we utilized r(CGG)99 repeats embedded in the 5′-untranslated region (5′-UTR) of the enhanced green fluorescence protein containing plasmid ($CGG\times_{99}$-EGFP-pcDNA3.1) that mimic the natural orientation of $r(CGG)^{exp}$ in the *FMR1* gene.

Molecule P5 reduced 60% of FMRpolyG aggregates at 25.0 µM and reduced them to 84% at 100.0 µM. Interestingly, no significant inhibition of EGFP and β-protein translation was found at the same concentration .

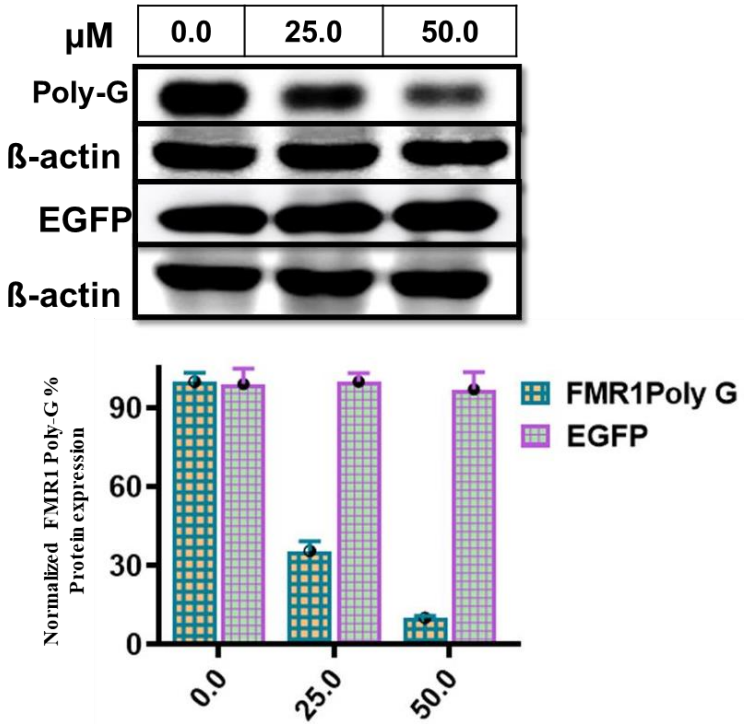

Figure 4.13: Immunoblots representing inhibition of FMR polyG protein aggregates for 24 h in the presence of P5, whereas no significant difference was seen in the concentration of protein controls.

4.8: Improvement of splicing defects in the cellular model

In the absence of r(CGG)^{exp}, *SMN2* exon 7 is included in 35% of mRNAs, while in the presence of r(CGG)^{exp}, the inclusion of *SMN2* exon 7 increases to 80% . Importantly, P5 at a concentration of 25.0 μM improves splicing defects of *SMN2* mRNA, and 50.0 μM P5 shows major improvement in pre-mRNA splicing defects. As a control, P5 does not show any significant effect on alternative splicing of *SMN2* in the absence of r(CGG)^{exp} .

Similarly, in Bcl-x gene, in the absence of r(CGG)^{exp} 45% of Bcl-xS RNA is present and 55 % of Bcl-Xl RNA is present, while in the presence of r(CGG)^{exp} 15% of Bcl-xS RNA is present and 85 % of Bcl-xL RNA is present. Importantly, P5 at a concentration of 25.0 μM

improves splicing defects of Bcl-x mRNA, and 50.0 μM P5 shows major improvement in pre-mRNA splicing defects. As a control, P5 does not show any significant effect on alternative splicing of Bcl-x in the absence of $r(CGG)^{exp}$.

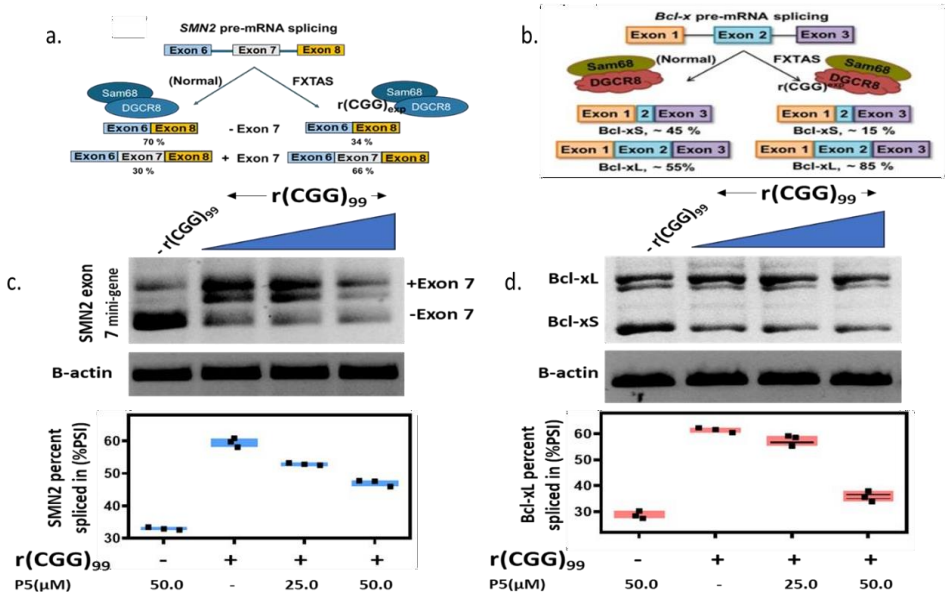

Figure 4.14: (a.) Schematic representation of splicing defects associated with the SMN2 (Survival of Motor Neuron 2) gene in FXTAS. (b.)Schematic representation of splicing defects associated with the Bcl-x (B-cell lymphoma extra large) gene in FXTAS. (c.) Gel images and graphs illustrate that P5 corrects the SMN2 defects in relation to their concentration. (d.) Gel images and graphs illustrate that P5 corrects the Bcl-x defects in relation to their concentration.

4.9: MitoSOX™ Red Staining in COS-7 Cells

MitoSOX staining shows a decrease in signal intensity on increasing concentration up to 50 μm. This denotes a reduction in Mitochondrial ROS production. The same is depicted by the pictures below.

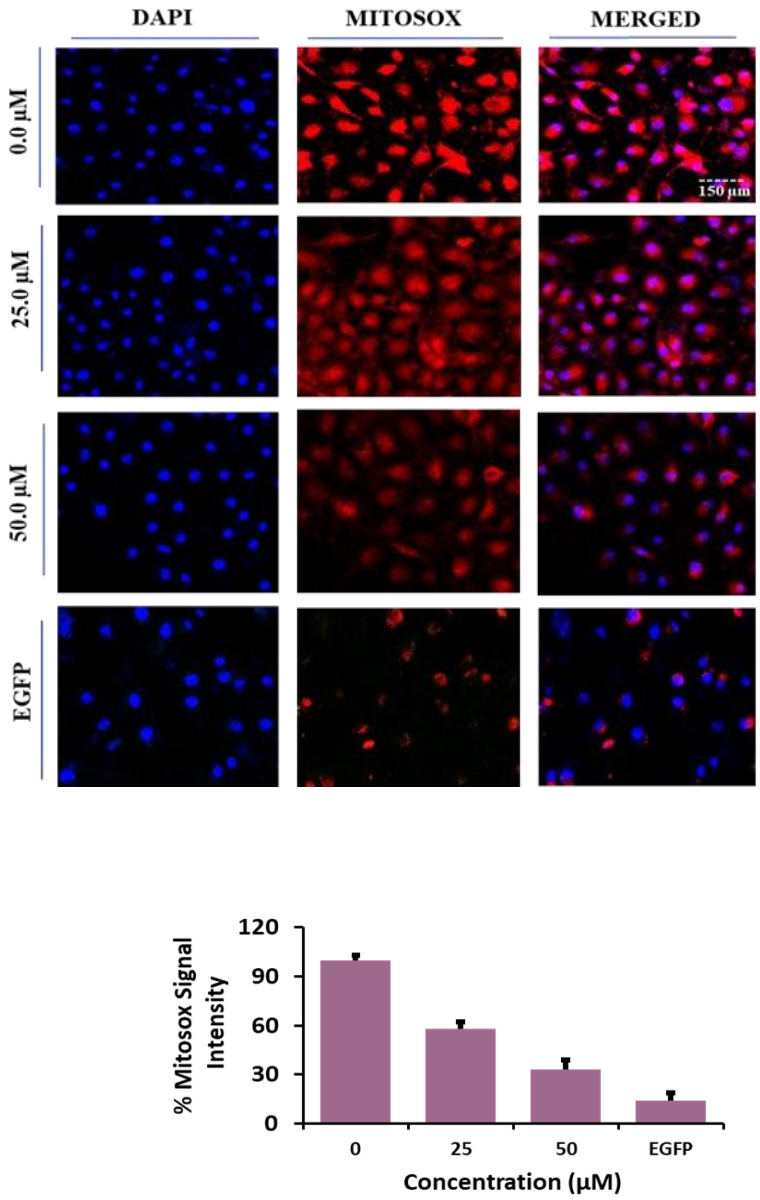

Figure 4.15: Fluorescence microscopy images of Cos7 cells after Mitosox staining. Accompanying Bar graph denoting percentage of Mitosox signal intensity.

4.10 : TMRM Staining in COS-7 Cells

TMRM staining shows increase in signal intensity on increasing concentration upto 50Mm. This denotes improvement in Mitochondrial membrane integrity. The same is depicted by the pictures below.

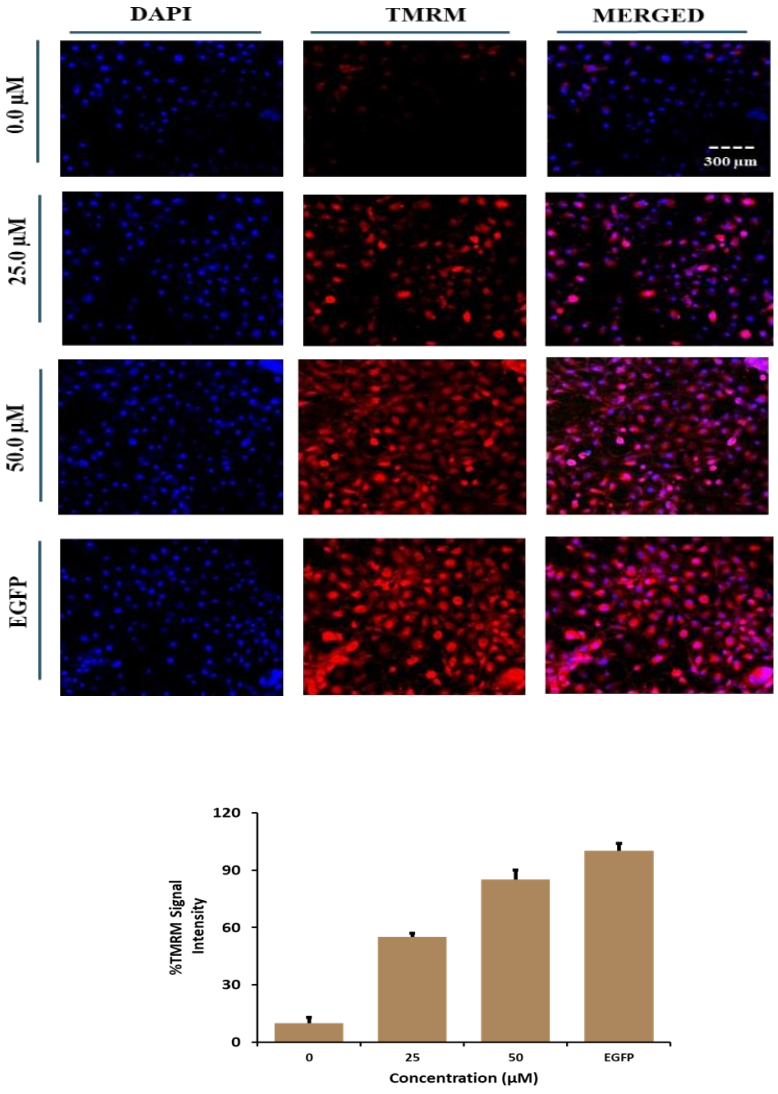

Figure 4.16: Fluorescence microscopy images of Cos7 cells after TMRM staining. Accompanying Bar graph denoting percentage TMRM signal intensity

4.11 : Rough eye phenotype assessment in *Drosophila* FXTAS model.

Approximately two-thirds of the genes in the *Drosophila melanogaster* genome play a role in the development of the eye. Thus, the expression of the FXTAS-associated mutant proteins through *GMR-GAL4* led to significant eye degeneration and noticeable external abnormalities in flies. Using the pan-retinal *GMR-GAL4* driver line, we induced the expression of *UAS-(CGG)$_{90}$-EGFP* and *UAS-EGFP* transgenes specifically within the compound eyes of *Drosophila*. We found that increasing concentrations of the P5 had no significant effect on rough eye phenotype, and loss of pigmentation in *(CGG)$_{90}$* flies. The control group expressing only EGFP also did not exhibit significant changes. P5 was administered via food at different concentrations. The results showed there is no improvement in eye phenotype upon drug administration. The following images show the same results.

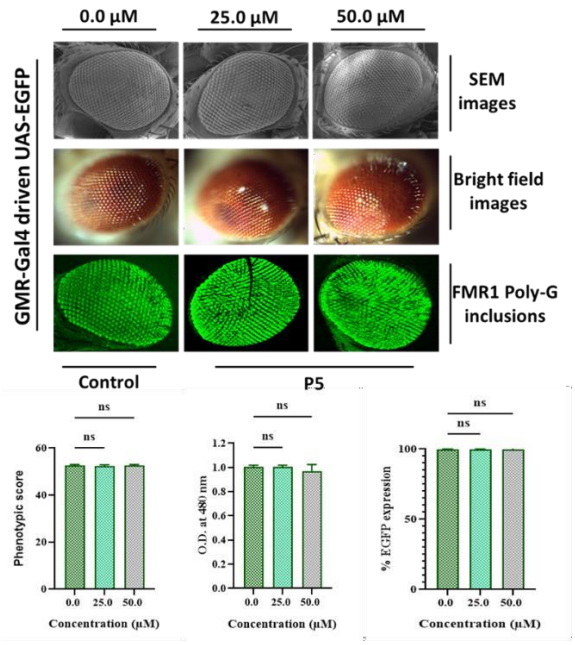

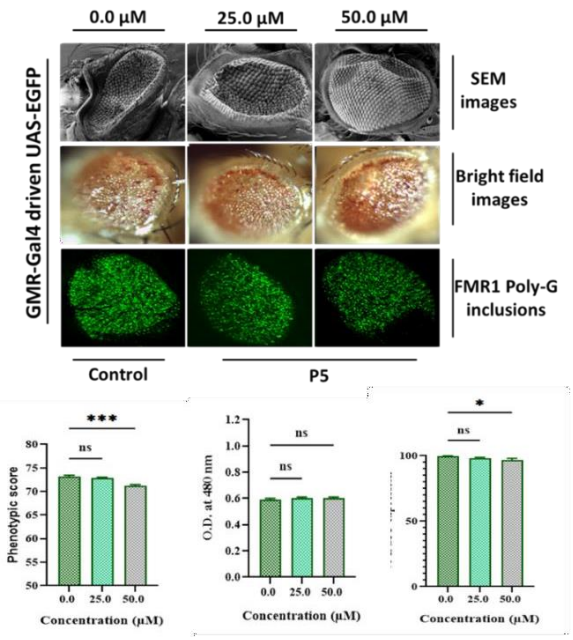

Figure 4.17: (a.) SEM, Light microscopic, and confocal images of the eyes of *GMR-Gal4 > UAS-EGFP* flies treated with different concentrations of P5. Bar graphs indicate the results of phenotypic score, eye pigmentation, and %EGFP expression, respectively, in the eyes of *GMR-Gal4 > UAS-EGFP* flies treated with different concentrations of P5. (b.) SEM, Light microscopic, and confocal images of the eyes of *GMR-Gal4 > UAS-(CGG)$_{90}$-EGFP* flies treated with different concentrations of P5. Bar graphs indicate the results of phenotypic score, eye pigmentation, and %EGFP expression, respectively, in the eyes of *GMR-Gal4 > UAS-EGFP* flies treated with different concentrations of P5.

4.12 : Drosophila larval Crawling assay

The Crawling assay result showed no significant improvement in locomotor functions. There was no difference in the distance crawled by diseased larvae and drug-treated larvae. The same results are shown below.

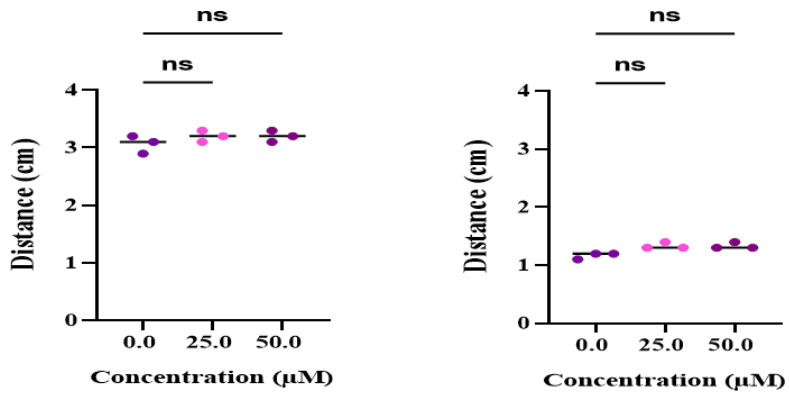

Figure 4.18: Crawling assay results for third-instar larvae (*Elav-Gal4 > UAS-(CGG)$_{90}$-EGFP*) treated with P5 assessing motor coordination and function

4.13. Drosophila Climbing assay

The Climbing assay result showed no significant increase in improvement of locomotor functions. There was no difference in the flight distance by diseased and drug treated flies. The same results are shown below.

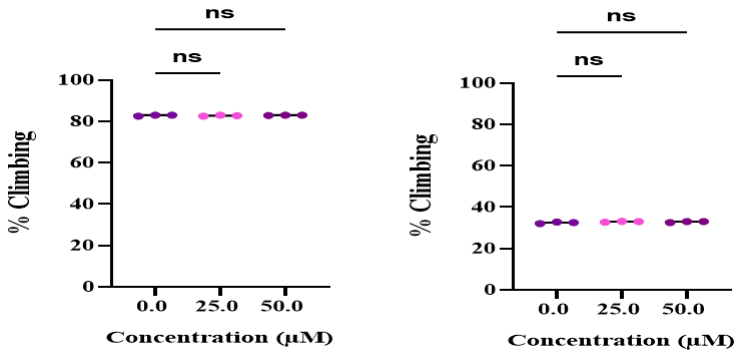

Figure 4.19: Climbing Assay for *Elav-Gal4 > UAS-(CGG)$_{90}$-EGFP* adult flies following the treatment with P5

4.14 : Drosophila Flight assay

The flight assay results revealed that treatment with the P5 did not lead to a noticeable improvement in the locomotor function of Drosophila. There was no significant increase in the average landing height compared to the untreated disease model group, indicating that the drug failed to rescue the flight impairment phenotype associated with the disorder. The same results are shown below.

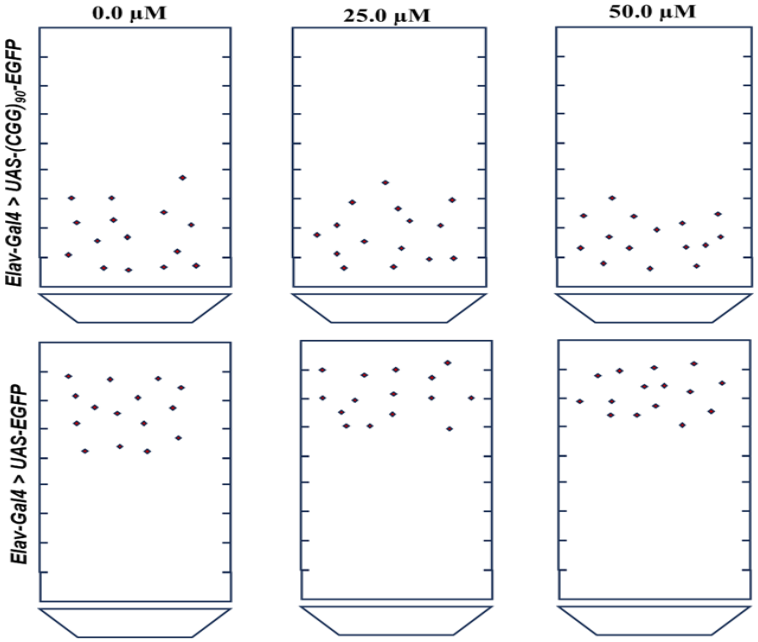

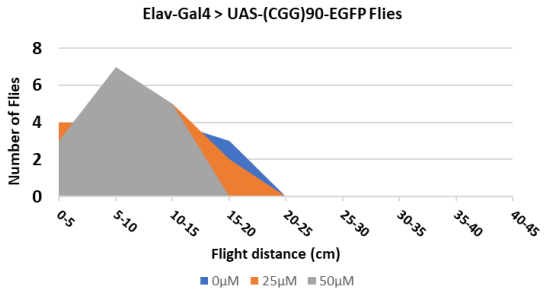

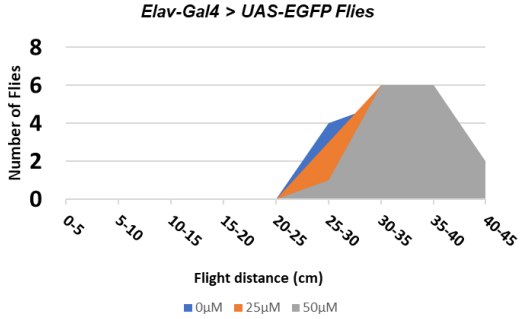

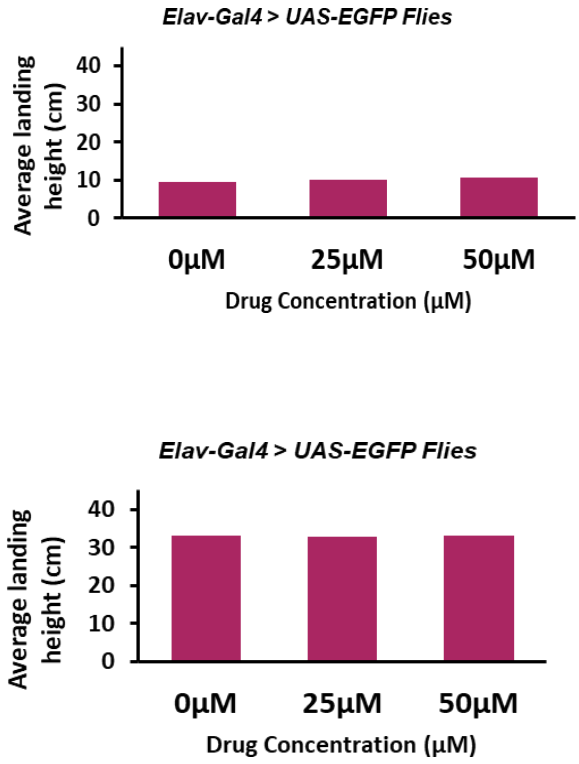

Figure 4.20: Schematic results of Drosophila flight assay. Accompanying area plot graphs indicate the number of flies at different heights of the flight chamber. The bar graph represents the average landing height of diseased (Elav-Gal4 > UAS-(CGG)90-EGFP) Flies and control *Elav-Gal4 > UAS-EGFP) Flies post treatment with varying concentration of P5.*

4.15: Quantification of RAN Translation by Western blot in *Drosophila* FXTAS model.

Consistent with the behavioral data from the flight assay, Western blot analysis further confirmed the lack of therapeutic efficacy of the tested drug. There was no observable reduction in the levels of FMR1-polyG protein in treated flies compared to the untreated disease model group. The absence of a decrease in polyG accumulation suggests that the drug failed to mitigate the toxic protein burden characteristic of FXTAS pathology. These findings collectively indicate that the compound did

not produce significant molecular or functional improvements in this model system.

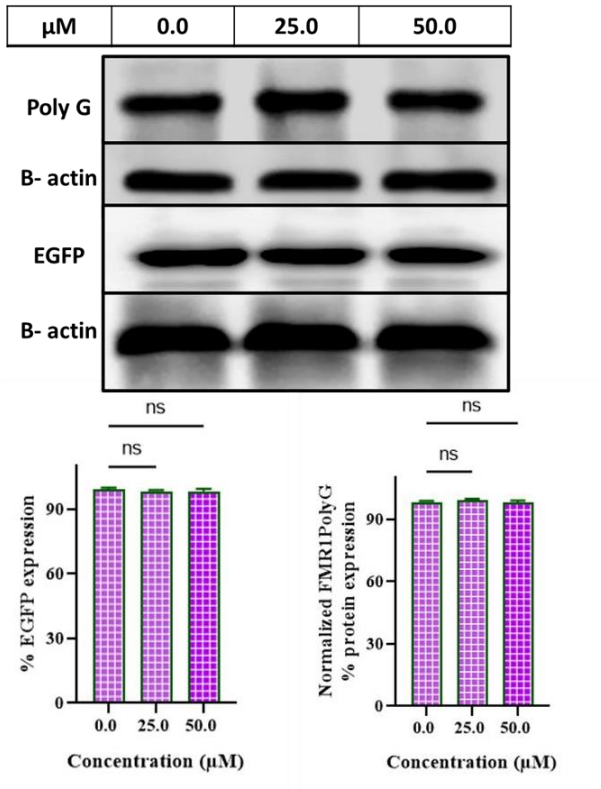

Figure 4.21: Immunoblots representing levels of Poly-G post drug treatment in *Drosophila* FXTAS model.

Chapter 5

Discussion

Fragile X-associated Tremor/Ataxia Syndrome (FXTAS) is a late-onset neurodegenerative disorder caused by a CGG trinucleotide repeat expansion in the 5′-UTR of the *FMR1* gene. This expansion leads to RNA toxic gain-of-function and the production of toxic repeat-associated non-AUG (RAN) translation products such as FMRpolyG, both of which contribute to disease pathology. In this study, we investigated the potential of a small molecule, designated P5, to target pathogenic r(CGG)^{exp} RNA structures and mitigate associated toxicity. Our multidisciplinary approach encompassed primary binding studies, biophysical characterization, in vitro cellular assays, and in vivo validation in *Drosophila* models of FXTAS. While P5 demonstrated promising results in vitro, its lack of efficacy in the *Drosophila* model highlights the challenges in translating therapeutic potential from cellular to organismal systems.

Biophysical Evidence of P5-RNA Binding

Initial assessments focused on the interaction between P5 and r(CGG)^{exp} motifs using biophysical techniques. Fluorescence titration assays revealed a high binding affinity of P5 toward r(CGG)$_6$ RNA, with a dissociation constant (K_d) in the low micromolar range. This strong interaction was further supported by circular dichroism (CD) spectroscopy, which showed a dose-dependent alteration in RNA secondary structure upon P5 binding. The observed changes in CD signals indicated that P5 likely intercalates or stacks within the repeat region, thereby altering the conformation of the RNA hairpins characteristic of expanded CGG repeats.

Additional confirmation came from the PCR stop assay, which revealed P5-induced polymerase stalling at the repeat region, suggesting the formation of a stable RNA-ligand complex.

Electrophoretic mobility shift assays (EMSA) also demonstrated a clear shift in RNA migration patterns upon P5 treatment, further substantiating its specific interaction with r(CGG)^{exp} sequences. Collectively, these biophysical experiments confirmed that P5 selectively binds to r(CGG)^{exp} RNA and modulates its structure, providing a mechanistic foundation for its downstream effects.

Cellular Effects of P5 in FXTAS Model Systems

Having validated the direct RNA-binding ability of P5, we sought to investigate its functional efficacy in a mammalian cell-based FXTAS model. We developed a reporter construct (CGG×99-EGFP-pcDNA3.1) where 99 CGG repeats were inserted into the 5′-UTR of an EGFP gene, mimicking the natural orientation of the *FMR1* transcript in FXTAS patients. Transfection of this plasmid led to the expression of r(CGG)^{exp} RNA and the production of toxic FMRpolyG proteins via RAN translation, thereby recapitulating key pathological features of the disease.

Upon treatment with P5, a substantial reduction in the number of FMRpolyG aggregates was observed. At 25 μM, P5 reduced the aggregate burden by approximately 60%, and this effect was further enhanced to 84% at 100 μM. Notably, these reductions occurred without any significant change in the expression of control proteins such as EGFP and β-actin, suggesting that P5 does not interfere with global protein translation. This selectivity is crucial for any therapeutic candidate, as nonspecific inhibition of translation can lead to unintended cytotoxicity. These results strongly support the notion that P5 disrupts the toxic RNA-protein interactions or blocks RAN translation specifically at r(CGG)^{exp} sites, thereby reducing cellular toxicity.

Additionally, immunofluorescence analysis confirmed a decrease in nuclear RNA foci, consistent with the disruption of pathogenic RNA structures by P5. These in vitro findings underscore the dual-action

potential of P5: remodeling RNA secondary structures to prevent protein sequestration and inhibiting the production of toxic polyglycine peptides.

Failure in *Drosophila* Model and Possible Explanations

Despite these encouraging results in cell-based models, P5 failed to produce a significant therapeutic effect in a *Drosophila melanogaster* model of FXTAS, which expresses 90 CGG repeats in neuronal tissues. The *Drosophila* model has been widely used for in vivo FXTAS research due to its ability to reproduce phenotypes such as neurodegeneration, locomotor deficits, and reduced lifespan, making it a robust system for preclinical validation.

In our in vivo experiments, P5 administration at various concentrations did not result in any noticeable improvement in phenotype, aggregate reduction, or lifespan extension. This disparity between in vitro efficacy and in vivo failure raises several important considerations.

First, pharmacokinetic limitations may underlie the lack of efficacy in *Drosophila*. P5 might have poor bioavailability, limited absorption through the cuticle or gut, or rapid metabolic degradation, resulting in sub-therapeutic concentrations at the target tissues. Without effective systemic exposure, the compound cannot exert its intended effect on neuronal $r(CGG)^{exp}$ RNA.

Second, differences in the cellular and molecular environment between mammalian cells and fly neurons may influence the behavior of both the RNA target and the compound. For instance, variations in RNA-binding protein availability, nuclear transport mechanisms, or RAN translation machinery might alter how $r(CGG)^{exp}$ is processed or how P5 interacts with it. These species-specific factors could reduce the compound's binding efficacy or diminish its downstream effects in *Drosophila*.

Third, the blood-brain barrier (BBB) equivalent in flies may restrict P5's entry into the nervous system. Although the *Drosophila* BBB differs structurally from mammals, it still functions as a selective permeability barrier, potentially limiting the drug's access to neuronal r(CGG)^{exp} RNA. Further studies using fluorescent or radiolabeled P5 derivatives could help assess its tissue distribution and CNS penetration in vivo.

Lastly, compound solubility and stability in the fly food medium may also play a role. If P5 precipitates or degrades in the delivery medium, its effective dose would be drastically reduced. Alternative delivery strategies, such as microinjection or encapsulation, may be necessary to circumvent these limitations in future experiments.

Chapter 6

Conclusion and Future Perspective

The study successfully employed a multi-tiered approach to evaluate the therapeutic potential of an FDA-approved small molecule against expanded CGG repeat RNA implicated in Fragile X-associated Tremor/Ataxia Syndrome (FXTAS). Initial biophysical assays, including fluorescence-based binding, circular dichroism (CD) spectroscopy, and electrophoretic mobility shift assays (EMSA), confirmed the specific interaction between the compound and r(CGG)exp RNA sequences. These interactions supported the hypothesis that the molecule could modulate RNA conformation and reduce its pathogenic effects. Further validation in cell-based assays revealed promising results: the compound reduced the number of nuclear RNA foci, corrected splicing abnormalities, and decreased the formation of polyG inclusions, indicating its ability to partially rescue cellular phenotypes associated with RNA toxicity.

However, despite these encouraging findings in vitro, the compound failed to demonstrate neuroprotective effects in the in vivo *Drosophila melanogaster* model of FXTAS. Behavioral assays, including flight and negative geotaxis tests, showed no significant improvement in motor coordination or climbing ability following treatment. Additionally, Western blot analysis did not show a reduction in the expression of FMR1-polyG protein, indicating persistent proteinopathy despite drug administration. These results highlight a critical translational gap between cellular and organismal models, emphasizing the complexity of addressing neurodegeneration in a whole-animal context.

Moving forward, several strategies can be pursued to overcome the current limitations. First, structural analogs of the tested compound can be synthesized and screened for improved potency, selectivity, and bioavailability. Second, delivery methods could be optimized to enhance drug penetration into neuronal tissues in vivo. Additionally,

combinatorial approaches involving RNA-targeting compounds and protein aggregation inhibitors may offer synergistic benefits. Expanding this research into mammalian models, such as transgenic mice, could further clarify the pharmacokinetic and pharmacodynamic profiles required for therapeutic efficacy. Finally, transcriptomic and proteomic studies may uncover compensatory pathways or off-target effects responsible for the lack of in vivo success, guiding the development of more refined therapeutic strategies for FXTAS and related repeat expansion disorders.

References

1- Ashburn, T. T., & Thor, K. B. (2004). Drug repositioning: Identifying and developing new uses for existing drugs. *Nature Reviews Drug Discovery*, *3*(8), 673–683. https://doi.org/10.1038/nrd1468

2- Benatar, M. (2007). Lost in translation: Treatment trials in the SOD1 mouse and in human ALS. *Neurobiology of Disease*, *26*(1), 1–13. https://doi.org/10.1016/j.nbd.2006.12.015

3- Bové, J., Martinez-Vicente, M., & Vila, M. (2011). The pharmacological manipulation of autophagy for the treatment of neurodegenerative diseases. *Trends in Pharmacological Sciences*, *32*(9), 475–483. https://doi.org/10.1016/j.tips.2011.06.005

4- Budworth, H., & McMurray, C. T. (2013). A brief history of triplet repeat diseases. In *Methods in Molecular Biology* (Vol. 1010, pp. 3–17). Humana Press. https://doi.org/10.1007/978-1-62703-411-1_1

5- Cleary, J. D., & Ranum, L. P. W. (2014). Repeat-associated non-ATG (RAN) translation: New starts in microsatellite expansion disorders. *Current Opinion in Genetics & Development*, *26*, 6–15. https://doi.org/10.1016/j.gde.2014.03.002

6- Colak, D., Zaninovic, N., Cohen, M. S., et al. (2014). Promoter-bound trinucleotide repeat mRNA drives epigenetic silencing in fragile X syndrome. *Science*, *343*(6174), 1002–1005. https://doi.org/10.1126/science.1245831

7- Cummings, J., Lee, G., Ritter, A., & Zhong, K. (2019). Alzheimer's disease drug development pipeline: 2019. *Alzheimer's & Dementia: Translational Research & Clinical Interventions*, *5*, 272–293. https://doi.org/10.1016/j.trci.2019.05.008

8- Doble, A. (1996). The pharmacology and mechanism of action of riluzole. *Neurology*, *47*(6 Suppl 4), S233–S241. https://doi.org/10.1212/WNL.47.6_Suppl_4.233S

9- Feigin, V. L., Vos, T., Alahdab, F., et al. (2020). Global burden of neurodegenerative diseases and the role of risk factors: A systematic review and meta-analysis. *The Lancet Neurology*, *19*(7), 475–483. https://doi.org/10.1016/S1474-4422(20)30148-X

10- Ferrante, R. J., Kubilus, J. K., Lee, J., et al. (2003). Histone deacetylase inhibition by sodium butyrate and suberoylanilide hydroxamic acid delays neurodegeneration in a transgenic mouse model of Huntington's disease. *The Journal of Neuroscience, 23*(28), 9418–9427. https://doi.org/10.1523/JNEUROSCI.23-28-09418.2003

11- Fiszer, A., & Krzyzosiak, W. J. (2013). RNA toxicity in polyglutamine disorders: Concepts, models, and progress of research. *Journal of Molecular Medicine, 91*(6), 683–691. https://doi.org/10.1007/s00109-013-1020-z

12- Galie, N., Ghofrani, H. A., Torbicki, A., et al. (2005). Sildenafil citrate therapy for pulmonary arterial hypertension. *New England Journal of Medicine, 353*(20), 2148–2157. https://doi.org/10.1056/NEJMoa050010

13- Hagerman, P. J., & Hagerman, R. J. (2001). Fragile X-associated tremor/ataxia syndrome (FXTAS). *Mental Retardation and Developmental Disabilities Research Reviews, 7*(4), 272–276. https://doi.org/10.1002/mrdd.1049

14- Hagerman, P., & Hagerman, R. (2016). Fragile X-associated tremor/ataxia syndrome – Features, mechanisms and management. *Nature Reviews Neurology, 12*(7), 403–412. https://doi.org/10.1038/nrneurol.2016.82

15- Heneka, M. T., Carson, M. J., Khoury, J. E., et al. (2014). Neuroinflammation in Alzheimer's disease. *The Lancet Neurology, 13*(4), 388–405. https://doi.org/10.1016/S1474-4422(14)70036-6

16- Jacquemont, S., Hagerman, R. J., Leehey, M. A., et al. (2003). Fragile X premutation tremor/ataxia syndrome: Molecular, clinical, and neuroimaging correlates. *American Journal of Human Genetics, 72*(4), 869–878. https://doi.org/10.1086/374321

17- Kalia, L. V., & Lang, A. E. (2015). Parkinson's disease. *The Lancet, 386*(9996), 896–912. https://doi.org/10.1016/S0140-6736(14)61393-3

18- Malik, I., Kelley, C. P., Wang, E. T., & Todd, P. K. (2021). Molecular mechanisms underlying nucleotide repeat expansion disorders. *Nature Reviews Molecular Cell Biology, 22*(9), 589–607. https://doi.org/10.1038/s41580-021-00364-6

19- Messenger, A. G., & Rundegren, J. (2004). Minoxidil: Mechanisms of action on hair growth. *British Journal of Dermatology, 150*(2), 186–194. https://doi.org/10.1111/j.1365-2133.2004.05785.x

20- Mullard, A. (2012). Sting of Alzheimer's failures offset by upcoming prevention trials. *Nature Reviews Drug Discovery, 11*(9), 657–660. https://doi.org/10.1038/nrd3814

21- Nosengo, N. (2016). Can you teach old drugs new tricks? *Nature, 534*(7607), 314–316. https://doi.org/10.1038/534314a

22- Phiel, C. J., Zhang, F., Huang, E. Y., et al. (2001). Histone deacetylase is a direct target of valproic acid, a potent anticonvulsant, mood stabilizer, and teratogen. *Journal of Biological Chemistry, 276*(39), 36734–36741. https://doi.org/10.1074/jbc.M101287200

23- Richardson, P. G., Barlogie, B., Berenson, J., et al. (2002). Immunomodulatory drug CC-5013 overcomes drug resistance and is well tolerated in patients with relapsed multiple myeloma. *Blood, 100*(9), 3063–3067. https://doi.org/10.1182/blood-2002-03-0957

24- Ross, C. A., & Poirier, M. A. (2004). Protein aggregation and neurodegenerative disease. *Nature Medicine, 10*(7), S10–S17. https://doi.org/10.1038/nm1066

25- Ramanan, V. K., & Saykin, A. J. (2013). Pathways to neurodegeneration: Mechanistic insights from GWAS in Alzheimer's disease, Parkinson's disease, and related disorders. *American Journal of Neurodegenerative Disease, 2*(3), 145–175.

26- Su, Y., Ryder, J., Li, B., et al. (2004). Valproic acid ameliorates neurodegeneration in a Huntington's disease mouse model. *The Journal of Neuroscience, 24*(24), 5748–5756. https://doi.org/10.1523/JNEUROSCI.1177-04.2004

27- Sofola, O. A., Jin, P., Qin, Y., et al. (2007). RNA-binding proteins hnRNP A2/B1 and CUGBP1 suppress fragile X CGG premutation repeat–induced neurodegeneration in a Drosophila model of FXTAS. *Neuron, 55*(4), 565–571. https://doi.org/10.1016/j.neuron.2007.07.020

28- Todd, P. K., Oh, S. Y., Krans, A., et al. (2013). CGG repeat–associated translation mediates neurodegeneration in fragile X-associated tremor/ataxia syndrome. *Neuron, 78*(3), 440–455. https://doi.org/10.1016/j.neuron.2013.03.026